Celestial Mechanics Notes Set 4: The Circular Restricted Three Body Problem

J.D. Mireles James

December 19, 2006

Contents

1 Introduction: Non-Inertial Frames and the Circular Restricted Three Body Problem

These notes introduce a reduction of general three Body dynamics which is often quite useful in applications and which is an active area of dynamical systems research in it's own right. The system models the motion of a small projectile in the field of two much larger primaries, whose relative motion is known. The equations of motion as well as the only know integral of motion for this reduction are derived. The system has five equilibrium points. The location of these are found and stability is investigated. The dynamics near these points is explored in both the linear and nonlinear cases. In addition we present some simulation results which highlight the rich global dynamics of the problem.

In the next section, the equations of motion for the Circular Restricted Three Body Problem (**CRTBP**) are derived. The differential equations will be derived in the most 'by hand' fashion imaginable, without the use of any machinery from the theory of Hamiltonian systems. The motivation for this is that even though a sophisticated theory of coordinate transformations exists for Hamiltonian systems, this theory is developed out of interest in applications and not for love of abstraction for abstraction for abstractions sake.

The motivation for the theory of canonical transformations comes precisely from problems in fluid and celestial mechanics such as the one considered here, and working the problem without leaning on any transformation theory suggests much of the development of the theory and highlights it's utility.

It's also valuable to see how the problem can be done with only ideas from elementary calculus and linear algebra. The derivation given here is the one you might do at your desk if you were sitting down to think about the problem for the first time (unless you are a Hamiltonian dynamists). The whole subject of transformation theory is enriched by working a few such examples. Similarly, the theory is unintelligible to someone who has never tried to work without it.

Often one begins with a problem in inertial (or "physical") coordinates having some natural symmetries which the inertial frame does not exploit. It is hoped that by changing coordinates to a more symmetrical frame the problem will be simplified. The motion of say, a spherical pendulum may be easier to understand when the equations of motion are expressed on the tangent bundle of a sphere rather than in $\mathbb{R}^6$ which is in some ways an un-natural frame for this problem. For example, the set of all possible configurations of the pendulum is a bounded set of measure zero in $\mathbb{R}^3$, so that somehow, $\mathbb{R}^3$ is an inefficient configuration space for this problem.

Further the change of reference may bring out connections to other problems, as the spherical pendulum in the nonlinear frame will be found to have the same equations of motion as a bead rolling without slipping in a spherical bowl.

Another such a problem is the **CRTBP** from celestial mechanics. To describe this system begin with two bodies m_1 and m_2 in circular orbits about their center of mass. A third body m_3 is introduced, whose mass is considered

to be negligible compared to the first two. Then it's presence does not disturbs the circular motion of the primary bodies.

This last statement will be made more precise later, but the physical intuition is that the situation is similar to that of a satellite in the gradational field of the earth and moon (whose orbits are almost circular) or an astroid in the field of Jupiter and the Sun. The model is idealized, but can make a fine starting point toward understanding more complicated configurations, such as a satellite in the Earth-Moon system perturbed by the Sun, or in the Earth-Moon System if the eccentricities of the primaries becomes important.

1.1 Derivation of the Equations of Motion for the Circular Restricted Three Body Problem

Begin by considering the equations of motion for the three body problem in an arbitrary inertial reference. We will use variables $\mathbf{r}_1$, $\mathbf{r}_2$, and $\mathbf{r}_3 \in \mathbb{R}^3$ for the positions of the three bodies, with masses m_1, m_2, m_3 respectively. With no loss of generality, suppose that $m_1 \geq m_2 \geq m_3$.

In the absence of any further simplifying assumptions the equations of motion are

$$\ddot{\mathbf{r}}_1 = G \left(\frac{m_2}{|\mathbf{r}_{12}|^3} \mathbf{r}_{12} + \frac{m_3}{|\mathbf{r}_{13}|^3} \mathbf{r}_{13} \right) \tag{1}$$

$$\ddot{\mathbf{r}}_2 = G \left(\frac{m_2}{|\mathbf{r}_{21}|^3} \mathbf{r}_{21} + \frac{m_3}{|\mathbf{r}_{23}|^3} \mathbf{r}_{23} \right) \tag{2}$$

$$\ddot{\mathbf{r}}_3 = G \left(\frac{m_1}{|\mathbf{r}_{31}|^3} \mathbf{r}_{31} + \frac{m_2}{|\mathbf{r}_{32}|^3} \mathbf{r}_{32} \right) \tag{3}$$

Where as always $\mathbf{r}_{ij} = \mathbf{r}_j - \mathbf{r}_i$ is the vector pointing from the tip of the vector $\mathbf{r}_i$ to the tip of the vector $\mathbf{r}_j$.

We are interested in a special situation. We suppose that the bodies at $\mathbf{r}_1$, and $\mathbf{r}_2$ are in circular motion about their center of mass. Call these the primary and secondary masses, also refereed to as the primaries.

We have established (in the first set of notes) that we can change coordinates so that the center of mass is at the origin and has zero velocity. Another linear change of variables brings the plane in which the primaries orbit to the xy-plane. These transformations do not change the equations of motion, they only change the initial conditions.

Now suppose that the third body is very small compared to both primaries. If it is small enough then it's effect on the primaries will be almost negligible, and we will assume that they stay in circular orbits about their center of mass. What we want to study is motion of the third body in the field generated by the primaries.

Note that the scalar m_3 appears only in equations (1) and (2). If we let m_3 go to zero, then these equations reduce to the equations of the two body

problem. Since we are assuming that the primaries evolve on circular orbits, we take $\mathbf{r}_1(t), \dot{\mathbf{r}}_1(t)$ and $\mathbf{r}_2(t), \dot{\mathbf{r}}_2(t)$ to be know.

Observe now that the equation of motion for the third body does not contain the scalar m_3 at all. This equation is unaffected when when we let m_3 go to zero, and it's still possible to make sense out the the dynamical system obtained by taking the limit as m_3 goes to zero. We simply consider the third body's evolution to be governed by non-autonomous second order nonlinear vector differential equation

$$\ddot{\mathbf{r}}_3 = G\left(\frac{m_1}{|\mathbf{r}_{31}|^3}\mathbf{r}_{31} + \frac{m_2}{|\mathbf{r}_{32}|^3}\mathbf{r}_{32}\right) \tag{4}$$

$$= G\left(\frac{m_1}{|\mathbf{r}_1(t) - \mathbf{r}_3|^3}[\mathbf{r}_1(t) - \mathbf{r}_3] + \frac{m_2}{|\mathbf{r}_2(t) - \mathbf{r}_3|^3}[\mathbf{r}_2(t) - \mathbf{r}_3]\right) \tag{5}$$

where $\mathbf{r}_1(t)$ and $\mathbf{r}_2(t)$ are known functions of time.

As it stands this equation is little better than the one we started with. A nonautonomous system of second order scalar *ODE's* is only marginally less headache than the original system of nine second order differential *ODE's* we began with. Especially as the original system was autonomous.

Even if we were to begin numerically experimenting with this system, we find the behavior often strange and lurching. Later we will show some trajectories of this system in these coordinates. The primary effect of these will be to highlight how much is actually gained by the coordinate change we are about to preform.

We will change to a rotating coordinate frame. This will have the advantage of fixing the position of the primaries and results in autonomous equations of motion. This in turn will allow fixed points in the dynamics. The down side is that the resulting frame is non-inertial. We will see that the trade off is worth it, and that it is possible to gain great insight into the dynamics of the system by this trick.

Lets assume that at time zero the primaries are on the x axis, this m_1 to the left of the origin (center of mass) at $-x_1$ and m_2 on the right at x_2, and that they rotate in a counterclockwise manor. Again, this can be done by a linear change of variables; a rotation and possibly a reflection, which change our initial conditions but not the form of the equations.

Now we will make a nonlinear change of variables which will change out equations (but incidentally leaves the initial conditions alone, as the transformation will be the identity at time zero). Define $R_\omega : \mathbb{R}^3 \times \mathbb{R} \to \mathbb{R}^3$ by

$$R_\omega(t) = \begin{pmatrix} \cos(\omega t) & \sin(\omega t) & 0 \\ -\sin(\omega t) & \cos(\omega t) & 0 \\ 0 & 0 & 1 \end{pmatrix}$$

and let the matrix act on vectors in $\mathbb{R}^3$ by matrix multiplication (so at each time the mapping is linear, in fact it's simply rotation by an angle $-\omega t$).

The transformation is ivertable with inverse

$$R_\omega^{-1}(t) = \begin{pmatrix} \cos(\omega t) & -\sin(\omega t) & 0 \\ \sin(\omega t) & \cos(\omega t) & 0 \\ 0 & 0 & 1 \end{pmatrix}$$

(it's a simple exercise to check that multiplying these two matrices together, in any order, yields the identity). But what is the effect of this transformation?

Imagine the untransformed system at time zero. The primaries are on the x-axis at $-x_1$ and x_2 with initial velocities pointing straight down and straight up respectively. Letting time begin to pass, the two bodies travel in counter-clockwise circular orbits around the origin. At time $\pi/2\omega$ they have moved $90°$ from their initial positions.

Applying $R_\omega(\pi/2\omega)$ to both $\mathbf{r}_2(\pi/2\omega)$ and $\mathbf{r}_1(\pi/2\omega)$ has the result of rotating each clockwise by $90°$, putting each back on the x axis at their original positions. And there is of course nothing nothing special about the time $\pi/2\omega$. We choose it to make the angles easy to visualize, but the same comments work for any time at all. Then R_ω has the effect of fixing the primaries to the x-axis, and is the transformation we seek.

Define the new variable $\mathbf{p} \in \mathbb{R}^3$ by

$$\mathbf{p} = \begin{bmatrix} x \\ y \\ z \end{bmatrix} = R_\omega(t) \begin{bmatrix} r_3^1 \\ r_3^2 \\ r_3^3 \end{bmatrix} = R_\omega(t)\mathbf{r}_3$$

where r_3^1, r_3^2, r_3^3 are the components of $\mathbf{r}_3$. In the new coordinates, the positions of the primaries are fixed. We now derive the equations of motion for the third body in these coordinates.

Again, we avoid the use canonical transformation theory and even fairly elementary results from physics about acceleration in rotation frames in favor of the most low tech method we can think of; we simply plug in and compute.

The inertial equation of motion for the third body is second order, so we note that $\mathbf{r}_3 = R_\omega(t)^{-1}\mathbf{p}$ and compute

$$\begin{aligned} \dot{\mathbf{r}}_3 &= \frac{d}{dt}[R_\omega^{-1}(t)\mathbf{p}] \\ &= \dot{R}_\omega^{-1}(t)\mathbf{p} + R_\omega^{-1}(t)\dot{\mathbf{p}} \end{aligned}$$

and from this

$$\begin{aligned} \ddot{\mathbf{r}}_3 &= \frac{d}{dt}\left(\dot{R}_\omega^{-1}(t)\mathbf{p} + R_\omega^{-1}(t)\dot{\mathbf{p}}\right) \\ &= \ddot{R}_\omega^{-1}(t)\mathbf{p} + 2\dot{R}_\omega^{-1}(t)\dot{\mathbf{p}} + R_\omega^{-1}(t)\ddot{\mathbf{p}} \end{aligned}$$

Note that this is the left hand side of the equations of motion for the third body.

To deal with the right hand side, note that $R_\omega(t)$ and it's inverse are both rotations, and hence preserve areas, and lengths. We can see this explicitly by computing

$$
\begin{aligned}
|\mathbf{r}_{ij}|^2 &= \mathbf{r}_{ij}^T \mathbf{r}_{ij} \\
&= [\mathbf{r}_j - \mathbf{r}_i]^T [\mathbf{r}_j - \mathbf{r}_i] \\
&= [R_\omega(t)^{-1}\mathbf{p}_j - R_\omega(t)^{-1}\mathbf{p}_i]^T [R_\omega(t)^{-1}\mathbf{p}_j - R_\omega(t)^{-1}\mathbf{p}_i] \\
&= [R_\omega(t)^{-1}(\mathbf{p}_j - \mathbf{p}_i)]^T [R_\omega(t)^{-1}(\mathbf{p}_j - \mathbf{p}_i)] \\
&= [\mathbf{p}_j - \mathbf{p}_i]^T [R_\omega(t)^{-1}]^T R_\omega(t)^{-1}[\mathbf{p}_j - \mathbf{p}_i] \\
&= [\mathbf{p}_j - \mathbf{p}_i]^T R_\omega(t) R_\omega(t)^{-1}[\mathbf{p}_j - \mathbf{p}_i] \\
&= [\mathbf{p}_j - \mathbf{p}_i]^T [\mathbf{p}_j - \mathbf{p}_i] \\
&= \mathbf{p}_{ij}^T \mathbf{p}_{ij} \\
&= |\mathbf{p}_{ij}|^2
\end{aligned}
$$

so that $|\mathbf{r}_{ij}| = |\mathbf{p}_{ij}|$. Here we have used the fact that $R_\omega(t)^T = R_\omega(t)^{-1}$ (this is obvious just by checking the definitions).

Then, making the substation $\mathbf{r}_3 = R_\omega(t)^{-1}\mathbf{p}$ in the right hand side of the equations of motion gives

$$
\begin{aligned}
G\left(\frac{m_1}{|\mathbf{r}_{31}|^3}\mathbf{r}_{31} + \frac{m_2}{|\mathbf{r}_{32}|^3}\mathbf{r}_{32}\right) &= G\left(\frac{m_1}{|\mathbf{p}_{31}|^3}R_\omega(t)^{-1}\mathbf{p}_{31} + \frac{m_2}{|\mathbf{p}_{32}|^3}R_\omega(t)^{-1}\mathbf{r}_{32}\right) \\
&= GR_\omega(t)^{-1}\left(\frac{m_1}{|\mathbf{p}_{31}|^3}\mathbf{p}_{31} + \frac{m_2}{|\mathbf{p}_{32}|^3}\mathbf{p}_{32}\right)
\end{aligned}
$$

Equating the transformed right and left hand sides gives

$$
\ddot{R}_\omega^{-1}(t)\mathbf{p} + 2\dot{R}_\omega^{-1}(t)\dot{\mathbf{p}} + R_\omega^{-1}(t)\ddot{\mathbf{p}} = GR_\omega(t)^{-1}\left(\frac{m_1}{|\mathbf{p}_{31}|^3}\mathbf{p}_{31} + \frac{m_2}{|\mathbf{p}_{32}|^3}\mathbf{p}_{32}\right)
$$

Here we are using $\mathbf{q}_{31}$ and $\mathbf{q}_{32}$ to denote $\mathbf{q}_1 - \mathbf{q}$ and $\mathbf{q}_2 - \mathbf{q}$ where we recall note that $\mathbf{q}_1$ is the coordinate vector of the primary body, and $\mathbf{q}_2$ is the coordinate vector of the secondary body, both in the rotating coordinates. Multiplying both sides by $R_\omega(t)$ this is

$$
R_\omega(t)\ddot{R}_\omega^{-1}(t)\mathbf{p} + 2R_\omega(t)\dot{R}_\omega^{-1}(t)\dot{\mathbf{p}} + R_\omega(t)R_\omega^{-1}(t)\ddot{\mathbf{p}} = G\left(\frac{m_1}{|\mathbf{p}_{31}|^3}\mathbf{p}_{31} + \frac{m_2}{|\mathbf{p}_{32}|^3}\mathbf{p}_{32}\right)
$$

or

$$
\ddot{\mathbf{p}} = -R_\omega(t)\ddot{R}_\omega^{-1}(t)\mathbf{p} - 2R_\omega(t)\dot{R}_\omega^{-1}(t)\dot{\mathbf{p}} + G\left(\frac{m_1}{|\mathbf{p}_{31}|^3}\mathbf{p}_{31} + \frac{m_2}{|\mathbf{p}_{32}|^3}\mathbf{p}_{32}\right)
$$

This is now a second order vector differential equation for the evolution of the third body in the rotating coordinate system. But it's nonautonomous and

at this point hard to consider an improvement over the initial equations. Then we consider the matrix product terms a little more carefully.

Again, we simply compute

$$
\begin{aligned}
R_\omega(t)\ddot{R}_\omega^{-1}(t) &= \begin{bmatrix} \cos(\omega t) & \sin(\omega t) & 0 \\ -\sin(\omega t) & \cos(\omega t) & 0 \\ 0 & 0 & 1 \end{bmatrix} \frac{d^2}{dt^2} \begin{bmatrix} \cos(\omega t) & -\sin(\omega t) & 0 \\ \sin(\omega t) & \cos(\omega t) & 0 \\ 0 & 0 & 1 \end{bmatrix} \\
&= \begin{bmatrix} \cos(\omega t) & \sin(\omega t) & 0 \\ -\sin(\omega t) & \cos(\omega t) & 0 \\ 0 & 0 & 1 \end{bmatrix} \frac{d}{dt} \left(-\omega \begin{bmatrix} \sin(\omega t) & \cos(\omega t) & 0 \\ -\cos(\omega t) & \sin(\omega t) & 0 \\ 0 & 0 & 1 \end{bmatrix} \right) \\
&= -\omega^2 \begin{bmatrix} \cos(\omega t) & \sin(\omega t) & 0 \\ -\sin(\omega t) & \cos(\omega t) & 0 \\ 0 & 0 & 1 \end{bmatrix} \begin{bmatrix} \cos(\omega t) & -\sin(\omega t) & 0 \\ \sin(\omega t) & \cos(\omega t) & 0 \\ 0 & 0 & 1 \end{bmatrix} \\
&= -\omega^2 R_\omega(t) R_\omega(t)^{-1} \\
&= -\omega^2 \mathbf{I}_{3\times3}
\end{aligned}
$$

Similarly

$$
\begin{aligned}
R_\omega(t)\dot{R}_\omega^{-1}(t) &= \begin{bmatrix} \cos(\omega t) & \sin(\omega t) & 0 \\ -\sin(\omega t) & \cos(\omega t) & 0 \\ 0 & 0 & 1 \end{bmatrix} \frac{d}{dt} \begin{bmatrix} \cos(\omega t) & -\sin(\omega t) & 0 \\ \sin(\omega t) & \cos(\omega t) & 0 \\ 0 & 0 & 1 \end{bmatrix} \\
&= -\omega \begin{bmatrix} \cos(\omega t) & \sin(\omega t) & 0 \\ -\sin(\omega t) & \cos(\omega t) & 0 \\ 0 & 0 & 1 \end{bmatrix} \begin{bmatrix} \sin(\omega t) & \cos(\omega t) & 0 \\ -\cos(\omega t) & \sin(\omega t) & 0 \\ 0 & 0 & 1 \end{bmatrix} \\
&= -\omega \begin{bmatrix} \cos(\omega t)\sin(\omega t) - \cos(\omega t)\sin(\omega t) & \cos^2(\omega t) + \sin^2(\omega t) & 0 \\ -\cos(\omega t)\sin(\omega t) + \cos(\omega t)\sin(\omega t) & -\cos^2(\omega t) - \sin^2(\omega t) & 0 \\ 0 & 0 & 0 \end{bmatrix} \\
&= -\omega \begin{bmatrix} 0 & 1 & 0 \\ -1 & 0 & 0 \\ 0 & 0 & 0 \end{bmatrix} \\
&= \begin{bmatrix} 0 & -\omega & 0 \\ \omega & 0 & 0 \\ 0 & 0 & 0 \end{bmatrix}
\end{aligned}
$$

At this point we should pause and admire our luck. Both of the matrix product terms reduce to constants. Since these were the nonautonomous terms in our *ODE's* the transformed equations will be autonomous. To write these equation in the most pleasing form expand the notation

$$
\mathbf{p}_{31} = \mathbf{p}_1 - \mathbf{p}_3 = \begin{bmatrix} -x_1 \\ 0 \\ 0 \end{bmatrix} - \begin{bmatrix} x \\ y \\ z \end{bmatrix} = -\begin{bmatrix} x_1 + x \\ y \\ z \end{bmatrix}
$$

and

7

$$\mathbf{p}_{32} = \mathbf{p}_2 - \mathbf{p}_3 = \begin{bmatrix} x_2 \\ 0 \\ 0 \end{bmatrix} - \begin{bmatrix} x \\ y \\ z \end{bmatrix} = -\begin{bmatrix} x - x_2 \\ y \\ z \end{bmatrix}$$

Then plugging all of this new information into the equations of motion yields

$$\ddot{\mathbf{p}} = \omega^2 \mathbf{I}_{3\times3} \mathbf{p} + 2 \begin{bmatrix} 0 & \omega & 0 \\ -\omega & 0 & 0 \\ 0 & 0 & 0 \end{bmatrix} \dot{\mathbf{p}} - G \left(\frac{m_1}{|\mathbf{p}_{31}|^3} \mathbf{p}_{31} + \frac{m_2}{|\mathbf{p}_{32}|^3} \mathbf{p}_{32} \right)$$

Or, upon writing the entire system in scalar form

$$\begin{bmatrix} \ddot{x} \\ \ddot{y} \\ \ddot{z} \end{bmatrix} = \begin{bmatrix} \omega^2 x + 2\omega\dot{y} - G\left(\frac{m_1}{r_1^3}(x+x_1) + \frac{m_2}{r_2^3}(x-x_2)\right) \\ \omega^2 y - 2\omega\dot{x} - G\left(\frac{m_1}{r_1^3}y + \frac{m_2}{r_2^3}y\right) \\ -G\left(\frac{m_1}{r_1^3}z + \frac{m_2}{r_2^3}z\right) \end{bmatrix}$$

where we define

$$r_1 = \sqrt{(x+x_1)^2 + y^2 + z^2}$$

and

$$r_2 = \sqrt{(x-x_2)^2 + y^2 + z^2}$$

The dynamical system defined by this system of equations will be referred to as the circular restricted three body problem in physical units.

1.2   Dimensionless Coordinates

Another set of reductions can be made if we make yet another coordinate change to dimensionless coordinates. Recall from our earlier discussion of two body dynamics that two bodies move in circular orbits if and only if the gravitational force balances the centrifugal acceleration. Then taking the plane of motion to be the xy-plane, we have

$$\omega = \sqrt{\frac{G(m_1 + m_2)}{r_{12}^3}} \tag{6}$$

where r_{12} is the distance between the two bodies. We have also take the center of mass to be fixed at the origin, with the heaver mass always on it's left a distance of x_1 and the lighter mass to it's right a distance of x_2 (these distances are constant as the motion is circular). If we make these into coordinates along the line between the masses, through the origin then the coordinates are $-x_1$ and x_2 as in the previous section.

In these coordinates, conservation of linear momentum gives us the single equation

$$-m_1 x_1 + m_2 x_2 = 0$$

which we solve to obtain

$$x_1 = \frac{m_2}{m_1} x_2$$

The distance between the primaries is $r_{12} = x_2 - (-x_1) = x_2 + x_1$.
Then $x_2 = r_{12} - x_1$ and we have

$$
\begin{aligned}
x_1 &= \frac{m_2}{m_1}(r_{12} - x_1) \\
\left(1 + \frac{m_2}{m_1}\right) x_1 &= \frac{m_2}{m_1} r_{12} \\
x_1 &= \frac{m_2/m_1}{1 + m_2/m_1} r_{12} \\
x_1 &= \frac{m_2}{m_1 + m_2} r_{12}
\end{aligned}
$$

A similar bit of algebra gives

$$x_2 = \left(1 - \frac{m_2}{m_1 + m_2}\right) r_{12}$$

We define the parameter

$$\mu = \frac{m_2}{m_1 + m_2}$$

and note that since $m_1 \geq m_2$, $0 < \mu \leq 1/2$ as m_2 is at most equal to m_1, in which case $\mu = 1/2$.

Now define a unit of distance (du) to be such that the primaries are a distance one apart;

$$r_{12} = 1 du$$

Next define mass units (mu) so that the total mass of the system is one;

$$m_1 + m_2 = 1 mu$$

We further define the time units to be such that the frequency of the system is 2π. In other words we want the primaries to make one revolution in 2π time units. This will force $\omega = 1 rad/tu$.

Then, in these units we have

$$1rad/tu = \omega = \sqrt{\frac{G(m_1 + m_2)}{r_{12}^3}} = \sqrt{\frac{G(1mu)}{(1du)^3}}$$

From here it is clear that the numerical value of G is one in these units.

Finally, note that since, by definition $\mu = \frac{m_2}{m_1+m_2}$ and in these units $m_1 + m_2 = 1$ we have that $m_2 = \mu$.

Using the same relation, solve instead for m_1;

$$
\begin{aligned}
\mu &= \frac{m_2}{m_1 + m_2} \\
\mu(m_1 + m_2) &= m_2 \\
m_1 &= \frac{m_2}{\mu} - m_2 \\
&= m_2(\frac{1}{\mu} - 1) \\
&= m_2\frac{1 - \mu}{\mu} \\
&= \mu\frac{1 - \mu}{\mu} \\
&= 1 - \mu
\end{aligned}
$$

Then in these special units both the locations, and masses of the primaries are expressed in terms of the parameter μ. To recapitulate, the primary body has mass $m_1 = 1 - \mu$ and is located at $-x_1 = -\mu$ in the rotating frame, while the secondary body has mass $m_2 = \mu$ and is located at $x_2 = 1 - \mu$ in the rotating frame. Furthermore $G = \omega = 1$.

Then is these "dimensional" units, the equations of motion are

$$
\begin{bmatrix} \ddot{x} \\ \ddot{y} \\ \ddot{z} \end{bmatrix} = \begin{bmatrix} x + 2\dot{y} - \frac{1-\mu}{r_1^3}[x + \mu] - \frac{\mu}{r_2^3}[x - (1 - \mu)] \\ y - 2\dot{x} - \frac{1-\mu}{r_1^3}y - \frac{\mu}{r_2^3}y \\ -\frac{1-\mu}{r_1^3}z - \frac{\mu}{r_2^3}z \end{bmatrix}
$$

with

$$r_1 = \sqrt{(x + \mu)^2 + y^2 + z^2}$$

and

$$r_2 = \sqrt{(x - (1 - \mu))^2 + y^2 + z^2}$$

The dynamical system defined by these equations is the dimensionless circular restricted three body problem, and is what we will refer to from now on as *the* **CRTBP**.

Define the function

$$U(x, y, z) = \frac{1}{2}(x^2 + y^2) + \frac{1 - \mu}{r_1} + \frac{\mu}{r_2}$$

Then it's easy to check that

$$\begin{bmatrix} \ddot{x} \\ \ddot{y} \\ \ddot{z} \end{bmatrix} = \begin{bmatrix} 2\dot{y} + \frac{\partial}{\partial x}U \\ -2\dot{x} + \frac{\partial}{\partial y}U \\ \frac{\partial}{\partial z}U \end{bmatrix}$$

Up till now we have written the system as a set of second order equations. But it is often useful to express the equations of motion as a vector field. This is easily done using the variable $\mathbf{p} = (x, y, z)$, and $\mathbf{q} = \dot{\mathbf{p}} = (\dot{x}, \dot{y}, \dot{z}) = (v_x, v_y, v_z) = (u, v, w)$. Then the vector field is

$$\begin{bmatrix} \dot{\mathbf{p}} \\ \dot{\mathbf{q}} \end{bmatrix} = \begin{bmatrix} \dot{x} \\ \dot{y} \\ \dot{z} \\ \dot{u} \\ \dot{v} \\ \dot{w} \end{bmatrix}$$

$$= \begin{bmatrix} u \\ v \\ w \\ 2\dot{y} + \frac{\partial}{\partial x}U \\ -2\dot{x} + \frac{\partial}{\partial y}U \\ \frac{\partial}{\partial z}U \end{bmatrix}$$

$$= f(\mathbf{p}, \mathbf{q})$$

where this last equality is meant to define the vector field $f : \mathbb{R}^6 \to \mathbb{R}^6$. If we let $\mathbf{x} \in \mathbb{R}^6$ be $\mathbf{x} = (\mathbf{p}, \mathbf{q})^T$ then $\dot{\mathbf{x}} = f(\mathbf{x})$ is convenient shorthand for the **CRTBP** vector field.

1.3   The Jacobi Energy: Integral of Motion

The **CRTBP** has one know integral of motion. The following derivation is the one most often given as it is quite elementary (even if it gives little insight. More illuminating derivations come can be given using more of the general theory of Hamiltonian systems). Begin with the scalar combination of dynamical variables $\ddot{x}\dot{x} + \ddot{y}\dot{y} + \ddot{z}\dot{z}$. Then observe that this is

$$\begin{aligned} \ddot{x}\dot{x} + \ddot{y}\dot{y} + \ddot{z}\dot{z} &= \dot{x}(2\dot{y} + U_x) + \dot{y}(-2\dot{x} + U_y) + \dot{z}(U_z) \\ &= \dot{x}U_x + \dot{y}U_y + \dot{z}U_z \end{aligned}$$

$$= D_t U(\mathbf{p(t)})$$

$$= \frac{d}{dt} U$$

Then we nonchalantly observe that

$$\frac{d}{dt} \frac{1}{2} (\dot{x}^2 + \dot{y}^2 + \dot{z}^2) = \ddot{x}\dot{x} + \ddot{y}\dot{y} + \ddot{z}\dot{z}$$

so that

$$\frac{d}{dt} \frac{1}{2} (\dot{x}^2 + \dot{y}^2 + \dot{z}^2) = \frac{d}{dt} U$$

Then

$$\frac{1}{2} (\dot{x}^2 + \dot{y}^2 + \dot{z}^2) = U(x, y, z) - C/2$$

where C is an arbitrary constant, and the minus sign and the factor of two are just a convention. Then it is the case that

$$2U(x, y, z) - (\dot{x}^2 + \dot{y}^2 + \dot{z}^2) = C$$

or

$$x^2 + y^2 + 2\frac{1-\mu}{r_1} + 2\frac{\mu}{r_2} - (\dot{x}^2 + \dot{y}^2 + \dot{z}^2) = C$$

This constant, or conserved, quantity is called the Jacobi Integral. Since it is a conserved quantity we often refer to it as the 'energy' or 'Jacobi energy'.

Note that $(\dot{x}^2 + \dot{y}^2 + \dot{z}^2) = |\mathbf{q}|^2$ is the square of velocity. Then if we fix an energy level, and an initial position (x_0, y_0, z_0) the magnitude of the velocity is determined, and remains constant throught the trajectory.

On the other hand, if we proscribe that the velocity be zero at a given energy, this will determine a set of initial conditions. These conditions implicitly solve the equation

$$x^2 + y^2 + 2\frac{1-\mu}{r_1} + 2\frac{\mu}{r_2} - C = 0$$

The solution set of this equation will be a two dimensional surface in the configuration space (the surface is not necessarily compact or connected) which can give much information about the possible dynamics at a given energy level.

This is due to the following; a trajectory which arrives at the zero velocity surface arrives, as the name suggests, with no velocity. Then, since it must stop there, it cannot go through or past it. So the zero velocity surface (or energy surface as we will sometimes call it) restricts the possible dynamics by telling you that some regions of phase space are unreachable at the given energy level. We will explore this idea in greater detail in a later section.

1.4 Existence and Location of the Libration Points

We want to compute the location of the collinear and equilateral libration points for this system. These are the roots of the equation $f(\mathbf{x}) = 0$. Then at any such point $u = v = w = 0$ (of course).

Consider first the collinear points. For these we have $y = z = 0$ and the vector equations reduces to

$$x - \frac{(1-\mu)(x+\mu)}{|x+\mu|^3} - \frac{\mu(x-1+\mu)}{|x-(1-\mu)|^3} = 0$$

The collinear libration points lie on the x-axis, along with the masses, which are located at $-\mu$ and $1-\mu$. Then these points are linearly ordered, and we have to consider the three cases $x < -\mu < 1 - \mu$, $-\mu < x < 1 - \mu$, and $-\mu < 1 - \mu < x$. In the first case we will denote the equilibrium by $x = L_3$, the second case $x = L_1$ and the third case $x = L_3$ (the reason for these names will be explained in a moment).

In the first case we have

$$|L + \mu| = -(L + \mu) \quad and \quad |L - (1-\mu)| = -(L - (1-\mu)) \tag{7}$$

as $L < -\mu$, and $L < 1 - \mu$ imply that $L + \mu < 0$ and $L - (1-\mu) < 0$. Then 7 becomes

$$L - \frac{(1-\mu)(L+\mu)}{(-1)(L+\mu)^3} - \frac{\mu(L-1+\mu)}{(-1)(L-(1-\mu))^3} = 0$$

or

$$\frac{L(L+\mu)^2(L-(1-\mu))^2 + (1-\mu)(L-(1-\mu))^2 + \mu(L+\mu)^2}{(L+\mu)^2(L-(1-\mu))^2} = 0$$

The left hand side is zero if and only if L is a root of the numerator. Expanding this gives the condition

$$L^5 + aL^4 + bL^3 + cL^2 + dL + e = 0$$

where

$$
\begin{aligned}
a &= 2(2\mu - 1) \\
b &= (1-\mu)^2 - 4\mu(1-\mu) + \mu^2 \\
c &= 2\mu(1-\mu)(1-2\mu) + 1 \\
d &= \mu^2(1-\mu)^2 + 2(\mu^2 - (1-\mu)^2) \\
e &= (1-\mu)^3 + \mu^3
\end{aligned}
$$

The polynomial is fifth order in L and there is no hope of an analytic solution. If we are working with the Earth-Moon system, μ is know and we can solve the equation numerically.

We have done just this, using MatLab's root finding capabilities (the program is 'hw4prob3' in the appendix). We find that the equation has a single real root

$$L_3 \approx -1.00511551160689$$

We have confirmed that this is indeed approximately an equilibrium point by simulating the system from the initial state $x = (-1.00511551160689, 0, 0, 0, 0, 0)$ we find that the trajectory is within 10^{-12} of the rest point after 50 months. (The period of the primaries is normalized to to 2π, but we know this to be one month. The simulation was run until $t_f = 50 * 6.282$ which is roughly 50 months).

Similar consideration of the remaining two cases show that L_1, and L_2 satisfy

$$L^5 + aL^4 + bL^3 + cL^2 + dL + e = 0$$

with

$$
\begin{aligned}
a &= 2(2\mu - 1) \\
b &= (1 - \mu)^2 - 4\mu(1 - \mu) + \mu^2 \\
c &= 2\mu(1 - \mu)(1 - 2\mu) + 1 \\
d &= \mu^2(1 - \mu)^2 + 2(\mu^2 + (1 - \mu)^2) \\
e &= (1 - \mu)^3 - \mu^3
\end{aligned}
$$

and

$$
\begin{aligned}
a &= 2(2\mu - 1) \\
b &= (1 - \mu)^2 - 4\mu(1 - \mu) + \mu^2 \\
c &= 2\mu(1 - \mu)(1 - 2\mu) - 1 \\
d &= \mu^2(1 - \mu)^2 + 2(\mu^2 - (1 - \mu)^2) \\
e &= -(1 - \mu)^3 - \mu^3
\end{aligned}
$$

respectively. Numerical solutions for these equations are found to be

$$L_1 \approx 0.83629259089993$$

$$L_2 \approx 1.15616816590553$$

Simulations of these states verify that these points are rest points as well.

The locations of the equilateral triangle libration points are much easier to compute, since they must lie at the vertex of an equilateral triangle whose base is the line between the two primaries. Since this line has length one, the distance from the primaries to either L_4 or L_5 must be one.

Since the base lies on the x-axis and the sides have length one we see that the height of the third vertex must be $y = \pm\sqrt{3}/2$. The x coordinate of either libration point must bisect the adjacent side. Since this side has length one, this coordinate must be $x = -\mu + 1/2$.

Using the μ value for the Earth-Moon system gives

$$L_4 \approx (0.48772252900000, 0.86602540378444)$$

and

$$L_5 \approx (0.48772252900000, -0.86602540378444)$$

We will see in the next section the these points are stable equilibria for the Earth-Moon system so simulation. Fig(1) shows the locations of the libration points found here.
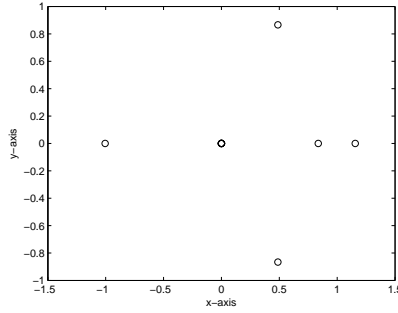
Figure 1: The Five Libration Points for the Earth-Moon System

2 Linearization of the CRTBP at the Libration Points

Recall again the equations of motion for the **CRTBP**;

$$
\begin{bmatrix} \dot{x} \\ \dot{y} \\ \dot{z} \\ \ddot{x} \\ \ddot{y} \\ \ddot{z} \end{bmatrix} = \begin{bmatrix} \dot{x} \\ \dot{y} \\ \dot{z} \\ \dot{u} \\ \dot{v} \\ \dot{w} \end{bmatrix} = \begin{bmatrix} u \\ v \\ w \\ x + 2\dot{y} - (1-\mu)\frac{x+\mu}{((x+\mu)^2+y^2+z^2)^{3/2}} - \mu\frac{x-(1-\mu)}{((x-(1-\mu))^2+y^2+z^2)^{3/2}} \\ y - 2\dot{x} - (1-\mu)\frac{y}{((x+\mu)^2+y^2+z^2)^{3/2}} - \mu\frac{y}{((x-(1-\mu))^2+y^2+z^2)^{3/2}} \\ -(1-\mu)\frac{y}{((x+\mu)^2+y^2+z^2)^{3/2}} - \mu\frac{y}{((x-(1-\mu))^2+y^2+z^2)^{3/2}} \end{bmatrix}
$$

$$
=
\begin{bmatrix}
u \\
v \\
w \\
2\dot{y} + D_x U \\
-2\dot{x} + D_y U \\
D_z U
\end{bmatrix}
$$

where $x, y, z \in \mathbb{R}^3$, $u = \dot{x}$, $v = \dot{y}$, $w = \dot{z}$ and

$$
U(x, y, z) = \frac{x^2 + y^2}{2} \frac{1 - \mu}{\sqrt{(x + \mu)^2 + y^2 +^2}} + \frac{\mu}{\sqrt{(x - (1 - \mu))^2 + y^2 + z^2}}
$$

(That the partials of U are indeed the terms in the equations of motion claimed here will be shown below.)

If we let $\mathbf{x} \in \mathbb{R}^6$ be the state vector $\mathbf{x} = (x, y, z, u, v, w)$ and $f : \mathbb{R}^6 \to \mathbb{R}^6$ be

$$
f(\mathbf{x}) =
\begin{bmatrix}
u \\
v \\
w \\
2\dot{y} + D_x U \\
-2\dot{x} + D_y U \\
D_z U
\end{bmatrix}
$$

then the libration points L_1, L_2, L_3, L_4, and L_5 are the zeros of f. The linearization about any of these points is

$$
\dot{\mathbf{x}} = D_{L_i} \mathbf{x}
$$

where D_{L_i} is the derivative of f evaluated at the libration point L_i. To compute this derivative let

$$
r_1 = \sqrt{(x + \mu))^2 + y^2 + z^2}
$$

$$
r_2 = \sqrt{(x - (1 - \mu))^2 + y^2 + z^2}
$$

Then we collect the following facts into a convenient lemma

Lemma 1 *Let x_i be the ith component of $\mathbf{x} = (x, y, z, u.v.w)$. Then*

$$
\frac{\partial}{\partial x_i} r_j =
\begin{cases}
(x + \mu)/r_1 & i = j = 1 \\
(x - (1 - \mu))/r_2 & i = 1, \ j = 2 \\
x_i / r_j & i = 2, 3, \ j = 1, 2 \\
0 & i = 4, 5, 6, \ j = 1, 2
\end{cases}
\tag{8}
$$

$$
\frac{\partial}{\partial x_i} \frac{1}{r_j} =
\begin{cases}
-\frac{x + \mu}{r_1^3} & i = j = 1 \\
-\frac{x - (1 - \mu)}{r_2^3} & i = 1, \ j = 2 \\
-\frac{x_i}{r_j^3} & i = 2, 3, \ j = 1, 2 \\
0 & i = 4, 5, 6, \ j = 1, 2
\end{cases}
\tag{9}
$$

$$\frac{\partial}{\partial x_i}\frac{1}{r_j^3} = \begin{cases} -3\frac{x+\mu}{r_1^5} & i = j = 1 \\ -3\frac{x-(1-\mu)}{r_2^5} & i = 1, \ j = 2 \\ -3\frac{x_i}{r_j^5} & i = 2, 3, \ j = 1, 2 \\ 0 & i = 4, 5, 6, \ j = 1, 2 \end{cases} \tag{10}$$

Proof These are all simple computations. When $i = 4, 5, 6$ the results are obvious as the r_j are functions of x_1, x_2, x_3 only. Now compute for example

$$\begin{aligned}
\frac{\partial}{\partial x_1}r_1 &= \frac{\partial}{\partial x}\sqrt{(x+\mu)^2 + y^2 + z^2} \\
&= \frac{\partial}{\partial x}((x+\mu)^2 + y^2 + z^2)^{1/2} \\
&= \frac{1}{2}((x+\mu)^2 + y^2 + z^2)^{-1/2}\frac{\partial}{\partial x}((x+\mu)^2 + y^2 + z^2) \\
&= \frac{1}{2}\frac{1}{((x+\mu)^2 + y^2 + z^2)^{1/2}}\frac{\partial}{\partial x}(x+\mu)^2 \\
&= \frac{1}{2}\frac{1}{((x+\mu)^2 + y^2 + z^2)^{1/2}}2(x+\mu) \\
&= \frac{x+\mu}{((x+\mu)^2 + y^2 + z^2)^{1/2}} \\
&= \frac{x+\mu}{r_1}
\end{aligned}$$

Nearly identical computations establish the rest of the cases for the first part of the lemma. For the second part we use the first and compute

$$\begin{aligned}
\frac{\partial}{\partial x_1}\frac{1}{r_1} &= \frac{\partial}{\partial x}r_1^{-1} \\
&= -r_1^{-2}\frac{\partial}{\partial x}r_1 \\
&= -\frac{1}{r_1^2}\frac{x+\mu}{r_1} \\
&= -\frac{x+\mu}{r_1^3}
\end{aligned}$$

and similarly for the other cases. The last part of the lemma is computed the same way;

$$\begin{aligned}
\frac{\partial}{\partial x_1}\frac{1}{r_1^3} &= \frac{\partial}{\partial x}r_1^{-3} \\
&= -3r_1^{-4}\frac{\partial}{\partial x}r_1
\end{aligned}$$

17

$$= -3\frac{1}{r_1^4}\frac{x+\mu}{r_1}$$

$$= -3\frac{x+\mu}{r_1^5}$$

$\square$

Using the previous lemma we can compute the partial derivatives of the components of the vector field f. The most involved part of this is the computation of the second partial derivatives of the potential function U, which we examine now;

$$
\begin{aligned}
\frac{\partial^2}{\partial x^2}U &= \frac{\partial}{\partial x}\frac{\partial}{\partial x}\left[\frac{x^2+y^2}{2}\frac{1-\mu}{r_1}+\frac{\mu}{r_2}\right] \\
&= \frac{\partial}{\partial x}\left[x+(1-\mu)\frac{\partial}{\partial x}\frac{1}{r_1}+\mu\frac{\partial}{\partial x}\frac{1}{r_2}\right] \\
&= \frac{\partial}{\partial x}\left[x-(1-\mu)\frac{x+\mu}{r_1^3}-\mu\frac{x-(1-\mu)}{r_2^3}\right] \\
&= 1-(1-\mu)\frac{\partial}{\partial x}\frac{x+\mu}{r_1^3}-\mu\frac{\partial}{\partial x}\frac{x-(1-\mu)}{r_2^3} \\
&= 1-(1-\mu)\left[\frac{1}{r_1^3}+(x+\mu)\frac{\partial}{\partial x}\frac{1}{r_1^3}\right]-\mu\left[\frac{1}{r_2^3}+(x-(1-\mu))\frac{\partial}{\partial x}\frac{1}{r_2^3}\right] \\
&= 1-(1-\mu)\left[\frac{1}{r_1^3}-3(x+\mu)\frac{x+\mu}{r_1^5}\right]-\mu\left[\frac{1}{r_2^3}-3(x-(1-\mu))\frac{x-(1-\mu)}{r_2^5}\right] \\
&= 1-(1-\mu)\left[\frac{1}{r_1^3}-3\frac{(x+\mu)^2}{r_1^5}\right]-\mu\left[\frac{1}{r_2^3}-3\frac{(x-(1-\mu))^2}{r_2^5}\right]
\end{aligned}
$$

A nearly identical calculation gives that

$$
\begin{aligned}
\frac{\partial^2}{\partial y^2}U &= \frac{\partial}{\partial y}\left[y-(1-\mu)\frac{y}{r_1^3}-\mu\frac{y}{r_2^3}\right] \\
&= 1-(1-\mu)\left[\frac{1}{r_1^3}-3\frac{y^2}{r_1^5}\right]-\mu\left[\frac{1}{r_2^3}-3\frac{y^2}{r_2^5}\right]
\end{aligned}
$$

and likewise that

$$
\begin{aligned}
\frac{\partial^2}{\partial z^2}U &= \frac{\partial}{\partial z}\left[-(1-\mu)\frac{z}{r_1^3}-\mu\frac{z}{r_2^3}\right] \\
&= -(1-\mu)\left[\frac{1}{r_1^3}-3\frac{z^2}{r_1^5}\right]-\mu\left[\frac{1}{r_2^3}-3\frac{z^2}{r_2^5}\right]
\end{aligned}
$$

18

At bare minimum these computations establish the fact claimed earlier; namely that the nonlinear terms in the vector field are given by the first partials of U. To compute the differential of f we will need the cross terms as well. These are $\frac{\partial^2}{\partial x \partial y}U$, $\frac{\partial^2}{\partial y \partial x}U$, $\frac{\partial^2}{\partial y \partial z}U$, $\frac{\partial^2}{\partial z \partial y}U$, $\frac{\partial^2}{\partial x \partial z}U$, and $\frac{\partial^2}{\partial z \partial x}U$. But equality of mixed partials reduces this to only three terms. We compute

$$
\begin{aligned}
\frac{\partial^2}{\partial x \partial y}U &= \frac{\partial}{\partial x}\frac{\partial}{\partial y}U \\
&= \frac{\partial}{\partial x}\frac{\partial}{\partial y}\left[\frac{x^2 + y^2}{2}\frac{1-\mu}{r_1} + \frac{\mu}{r_2}\right] \\
&= \frac{\partial}{\partial x}\left[y - (1-\mu)\frac{y}{r_1^3} - \mu\frac{y}{r_2^3}\right] \\
&= -(1-\mu)\frac{\partial}{\partial x}\frac{y}{r_1^3} - \mu\frac{\partial}{\partial x}\frac{y}{r_2^3} \\
&= -(1-\mu)y\frac{\partial}{\partial x}\frac{1}{r_1^3} - \mu y\frac{\partial}{\partial x}\frac{1}{r_1^3} \\
&= 3(1-\mu)y\frac{x+\mu}{r_1^5} + 3\mu y\frac{x-(1-\mu)}{r_2^5}
\end{aligned}
$$

Similarly

$$
\frac{\partial^2}{\partial x \partial z}U = 3(1-\mu)z\frac{x+\mu}{r_1^5} + 3\mu z\frac{x-(1-\mu)}{r_2^5}
$$

and

$$
\frac{\partial^2}{\partial y \partial z}U = 3(1-\mu)y\frac{z}{r_1^5} + 3\mu y\frac{z}{r_2^5}
$$

Now we want to evaluate all nine of these terms at the collinear libration points L_1, L_2, L_3. For these points it is the case that $z = y = 0$. Then at L_i, $i = 1, 2, 3$ we have

$$
r_1 = \sqrt{(L_i + \mu)^2 + 0^2 + 0^2} = \sqrt{(L_i + \mu)^2} = L_i + \mu
$$

$$
r_1 = \sqrt{(L_i - (1-\mu))^2 + 0^2 + 0^2} = \sqrt{(L_i - (1-\mu))^2} = L_i - (1-\mu)
$$

Then, evaluating the above expressions at L_i and a little algebra gives

$$
\frac{\partial^2}{\partial x^2}U|_{L_i} = 1 + 2\alpha
$$

19

$$\frac{\partial^2}{\partial y^2} U|_{L_i} = 1 - \alpha$$

$$\frac{\partial^2}{\partial z^2} U|_{L_i} = -\alpha$$

where

$$\alpha = \frac{1 - \mu}{|L_i + \mu|^3} + \frac{\mu}{|L_i - (1 - \mu)|^3}$$

and that all the mixed partials are zero, as $y = z = 0$.

We are ready to compute the differential. Write

$$f(\mathbf{x}) = \begin{bmatrix} f_1 \\ f_2 \\ f_3 \\ f_4 \\ f_5 \\ f_6 \end{bmatrix} = \begin{bmatrix} u \\ v \\ w \\ x + 2\dot{y} + D_x U \\ y - 2\dot{x} + D_y U \\ D_z U \end{bmatrix}$$

so that the differential is

$$D_{\mathbf{x}} f = \left(\frac{\partial}{\partial x_j} f_i \right)_{ij} = \begin{pmatrix} A & B \\ D_{\mathbf{x}}^2 U & C \end{pmatrix}$$

The sub-matrix A is the 6×6 matrix of partial derivatives of $f_1 = u, f_2 = v, f_3 = w$ with respect to the variables x, y, z. Since these are all zero, A is a matrix of zeros. Likewise the 6×6 matrix B is the identity, as its entries are the partial derivatives of the same terms, but now with respect to themselves. Then only the self partials are non-zero. In fact they are of course unity as $\partial x_i / \partial x_i$ is always one.

C is the 6×6 matrix of partials of f_4, f_5, and f_6 with respect to the velocity variables (u, v, w). f_3 depends only on x, y, z so the last row of C is zero. f_1 contains a $v = \dot{y}$ term while f_2 has a term containing $u = \dot{x}$. These dependencies are however linear, so C is a constant matrix.

Lastly, the bottom left 6×6 is the Hessian derivative of U. The terms of the differential have been computed throughout the section. Explicitly, the differential $D_{\mathbf{x}} f$ which governs the linear flow near the collinear libration points is

$$D_{\mathbf{x}} f = \begin{pmatrix} 0 & 0 & 0 & 1 & 0 & 0 \\ 0 & 0 & 0 & 0 & 1 & 0 \\ 0 & 0 & 0 & 0 & 0 & 1 \\ 1 + 2\alpha & 0 & 0 & 0 & 2 & 0 \\ 0 & 1 - \alpha & 0 & -2 & 0 & 0 \\ 0 & 0 & -\alpha & 0 & 0 & 0 \end{pmatrix} \tag{11}$$

20

as we have now computed.

At the equilateral triangle libration points the above is changed only slightly. At these points we have $r_1 = r_2 = 1$. The x and y coordinates of these equilibria are $x = -\mu + 1/2$ and $y = \pm\sqrt{3}/2$ Using this data yields, for L_i, $i = 4, 5$;

$$\frac{\partial^2}{\partial x^2}U|_{L_i} = 3/4$$

$$\frac{\partial^2}{\partial y^2}U|_{L_i} = 9/4$$

$$\frac{\partial^2}{\partial z^2}U|_{L_i} = -1$$

$$\frac{\partial^2}{\partial x \partial y}U|_{L_i}\frac{\partial^2}{\partial y \partial x}U|_{L_i} = \frac{3\sqrt{3}}{4}(1 - 2\mu)$$

and

$$\frac{\partial^2}{\partial x \partial z}U|_{L_i} = \frac{\partial^2}{\partial z \partial x}U|_{L_i} = \frac{\partial^2}{\partial y \partial z}U|_{L_i} = \frac{\partial^2}{\partial z \partial y}U|_{L_i} = 0$$

so that the linearized dynamics at the equilateral triangle libration points is

$$D_{\mathbf{x}}f = \begin{pmatrix} 0 & 0 & 0 & 1 & 0 & 0 \\ 0 & 0 & 0 & 0 & 1 & 0 \\ 0 & 0 & 0 & 0 & 0 & 1 \\ 3/4 & \frac{3\sqrt{3}}{4}(1-2\mu) & 0 & 0 & 2 & 0 \\ \frac{3\sqrt{3}}{4}(1-2\mu) & 9/4 & 0 & -2 & 0 & 0 \\ 0 & 0 & -1 & 0 & 0 & 0 \end{pmatrix}$$

With these matrices we can integrate the linearized vector field near any of the equilibria. The results give information about the dynamics near these points.

2.1 Stability of the Collinear Libration Points

The linearization of the vector field near the equilibria allows us to do more than just integrate the linear equations. Stability analysis of the linear system can tell us a great deal about the possible dynamics near these points. As an example we consider again the system matrix (13).

To determine the stability of the linear system we must find the eigenvectors and eigenvalues of $D_{\mathbf{x}}f$. Recall that λ is an eigenvalue if and only if

$$\det(D_{\mathbf{x}}f - \lambda\mathbf{I}) = 0 \tag{12}$$

A long calculation leads to the characteristic equation

$$\lambda^6 + 2\lambda^4 + (1 + 3\alpha - 3\alpha^2)\lambda^2 + \alpha(1 + \alpha - 2\alpha^2) = 0$$

Making the substitution $s = \lambda^2$ reduces this to

$$s^3 + 2s^2 + (1 + 3\alpha - 3\alpha^2)s + \alpha(1 + \alpha - 2\alpha^2) = 0$$

The resulting third order polynomial can be solved explicitly by, for example by the method of del Ferro [Nah], or by any computer algebra package. In any event, one finds that the roots are

$$
\begin{aligned}
s_1 &= -\alpha \\
s_2 &= \frac{1}{2}\sqrt{-4 + 2\alpha^2 + 2(9\alpha^2 - 8\alpha)} \\
s_3 &= \frac{1}{2}\sqrt{-4 + 2\alpha^2 - 2(9\alpha^2 - 8\alpha)}
\end{aligned}
$$

and the six eigenvalues are $\lambda_{k_{1,2}} = \pm(s_k)^{1/2}$, $k = 1, 2, 3$.

Consider the pair

$$\lambda_{1,2} = \pm\sqrt{-\alpha} = \pm\sqrt{-\frac{1-\mu}{(L_i + \mu)^3} - \frac{\mu}{(L_i - (1 - \mu))^3}}$$

If $\alpha < 0$ then $\lambda_{1,2}$ are real, with one positive and one negative. Then the corresponding eigenmodes have one exponentially decaying, and one exponentially growing term. The resulting solution is then unstable (in the sense of Lyapunov). Then the pressing question is, under what condition is $\alpha \geq 0$?

We are interested in the sign of

$$\alpha = \frac{1-\mu}{(L_i + \mu)^3} + \frac{\mu}{(L_i - (1 - \mu))^3} = \frac{(1-\mu)((L_i - (1 - \mu))^3) + \mu((L_i + \mu)^3)}{(L_i + \mu)^3(L_i - (1 - \mu))^3}$$

This is zero if and only if the numerator is.

2.2 Numerical Study of the Linear Stability of the Libration Points of the Planar Earth-Moon System

In Section 2 we computed the linearized vector fields about each of the libration points. Using those results and the coordinates of the libration points determined in the previous subsection, we can compute all the entries to the system matrix of the linear system. Here we consider only planar dynamics, so the matrices become

$$
D_{\mathbf{x}}f = \begin{pmatrix} 0 & 0 & 1 & 0 \\ 0 & 0 & 0 & 1 \\ 1 + 2\alpha & 0 & 0 & 2 \\ 0 & 1 - \alpha & -2 & 0 \end{pmatrix}
\tag{13}
$$

22

for the collinear points and,

$$D_{\mathbf{x}}f = \begin{pmatrix} 0 & 0 & 1 & 0 \\ 0 & 0 & 0 & 1 \\ 3/4 & \frac{3\sqrt{3}}{4}(1-2\mu) & 0 & 2 \\ \frac{3\sqrt{3}}{4}(1-2\mu) & 9/4 & -2 & 0 \end{pmatrix}$$

for the equilateral points

Consider the linear problem at L_1. Using μ for the Earth-Moon system and plugging the coordinates for L_1 into the system matrix gives a constant, whose eigenvalues are

$$\begin{aligned} \lambda_1 &= -2.93362180133514 \\ \lambda_2 &= 2.93362180133514 \\ \lambda_3 &= 0 - 2.33537262850121i \\ \lambda_4 &= 0 + 2.33537262850121i \end{aligned}$$

which is the classical "center $\times$ saddle" behavior we expect at L_1. The linear analysis tells us that L_1 has a one dimensional stable direction (manifold), and one dimensional unstable direction (manifold), and a two dimensional center (manifold). Then we expect to find that a generic solution near L_1 exhibits saddle behavior; limiting to L_1 in neither forward or backward time.

However the existence of stable, unstable, and center manifolds tells us that we should be able to find special solutions which either converge to, emanate from, or periodically orbit L_1.

Moreover, note that for every stable direction there is an unstable direction, and that the contraction rate of the first is exactly the expansion rate of the second. This keeps with our intuition that the system (which is Hamiltonian) preserves phase space volume.

Repeating this analysis at L_2 and L_3 gives

$$\begin{aligned} \lambda_1 &= -2.15752304760904 \\ \lambda_2 &= 2.15752304760904 \\ \lambda_3 &= 0 - 1.86197217347509i \\ \lambda_4 &= 0 + 1.86197217347509i \end{aligned}$$

and

$$\begin{aligned} \lambda_1 &= 0 - 1.89143870748167i \\ \lambda_2 &= 0 + 1.89143870748167i \\ \lambda_3 &= 0.75487708109713 \\ \lambda_4 &= -0.75487708109713 \end{aligned}$$

respectively. We see that L_2 and L_3 have the same stability types as L_1. Of the three systems, L_1 has the strongest expansion and contraction rates, while L_3 has the least. L_1 has the highest linearized frequency and L_3 the lowest.

About L_4 and L_5 the eigenvalues of the linearized system are

$$
\begin{aligned}
\lambda_1 &= -0.95396766945875i \\
\lambda_2 &= 0.95396766945875i \\
\lambda_3 &= -0.29990946238396i \\
\lambda_4 &= 0.29990946238396i
\end{aligned}
$$

and we have "center $\times$ center" dynamics for the linear system. Here there are no stable, and unstable manifolds. Instead there are two distinct linear frequencies. All the motion beginning near enough to L_4 or L_5 stays near them. We expect to see many bounded orbits, and possibly be able to find periodic ones, near these points, (although it's harder to say for sure. The relationship between the linear dynamics on a center, and the nonlinear dynamics in the center manifold can be dubious. In fact it can be advantageous and even necessary to consider the normal form near such a non-hyperbolic fixed point in order to get a topological conjugacy. Here we are only trying to get rough ideas about what is going on, and we will see that in fact we get very good information from this linear analysis.)

Already then the linear flow near the libration points has increased our understanding of the dynamics of the problem

3 Zero Velocity Surfaces in the Earth-Moon System

The next two subsections examine the zero velocity curves and surfaces in the planar and spatial **CRTBP** respectively. These curves and surfaces are obtained by choosing an energy level, setting the velocity terms in the Jacobi Integral to zero, and plotting the implicitly defined curve or surface so defined. The physicial/dynamical significance of the resulting varieties is as follows; once an energy level is fixed, the magnitude of the velocity at any point is uniquely determined.

If an orbit begins from a give point with this velocity, then should it reach the Jacobi Surface it's velocity must be zero when it arrives. Then it cannot pass through the surface. In this way, the Jacobi surfaces determine the allowable regions of motion for fixed energies in the **CRTBP**. These allowable regions are called *Hill's Regions*.

3.1 The Zero Velocity Curves in the Planar Problem

We can compute the Jacobi constants at each libration point now as well. Since a trajectory at any libration point is a fixed point, such a trajectory is a zero

velocity point. Then we expect each libration point to lie on the Jacobi surface (zero velocity curve) at it's own Jacobi energy.

We compute

$$
\begin{aligned}
J(L_1) &= C_1 = 3.18950841737352 \\
J(L_2) &= C_2 = 3.17315916582532 \\
J(L_3) &= C_3 = 3.01227396009323 \\
J(L_4) &= C_4 = 2.98787326529416 \\
J(L_5) &= C_5 = 2.98787326529416
\end{aligned}
$$

and plot the associated zero energy curves.

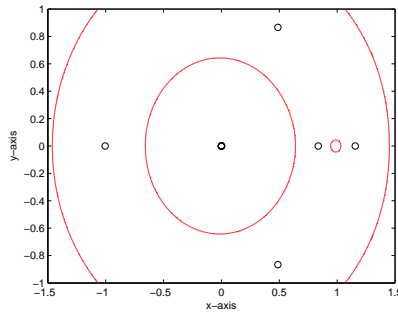Consider first Fig(2). This is the zero velocity curve for an energy $1.1C_1$ just above the energy of L_1

Figure 2: Zero velocity curve at 1.1 C_1

At this energy level the allowable orbits live in three disconnected domains. A body orbiting the Earth cannot find it's way to the Moon, and vice a versa. A body far from the center of mass can never arrive at the earth or the moon. Note also that for orbits in the connected component of the Earth or the Moon, only bounded motions are possible.

Now we consider the zero velocity curve at $C = 1.001C_1$, an energy larger than the energy of L_1, but now only marginally. This is shown in Fig(3).

At this energy the Earth and Moon still live in disconnected components, however the Moons component is growing and the barrier between the Earth and Moon is shrinking. The black circle on the left is L_1. We can see that it still lies in the inaccessible region, but only just barely.

The next plot, Fig(4) shows the zero velocity curve at the energy level of L_1.

The plot suggests (and it is in fact the case) that the barrier between the Earth and the Moon is just opening at the energy C_1. This is the reason for the name L_1. It is the first point where the Jacobi surface begins to "tear".
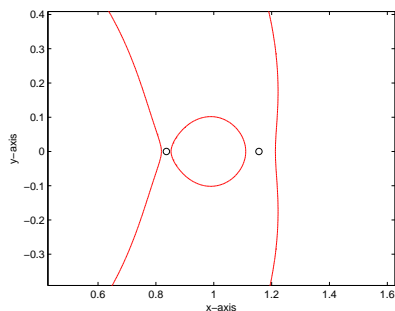
Figure 3: Zero velocity curve at 1.001 C_1
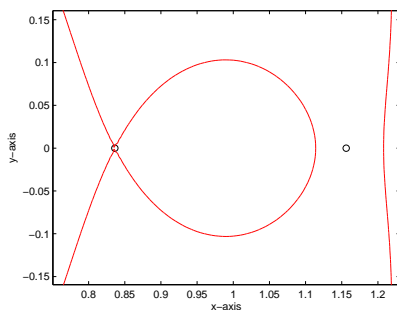
Figure 4: Zero velocity curve at C_1

Actually at this energy the two domains are still disconnected at this energy, as no orbit can go through the fixed point at L_1. But any lessening of the energy will allow passage as we see in the next plot.

In Fig(5 we see that the barrier between the Earth and the Moon has now reseeded, and there is a "neck" near L_1 through which a trajectory might pass. In fact the linearized dynamics at L_1 show it to be a fixed point of "center $\times$ saddle" type, and while most orbits will be ejected from this neck, the presence of the center manifold in the nonlinear problem suggests that we may be able to find periodic orbits in the neck, which orbit L_1. We can also see in this figure that a dimple is forming in the Jacobi surface near L_2.

Then we shift our attention away from $L1$ and consider L_2. As it's name suggests and Fig() shows, the Jacobi surface will open again at the point $(L_2, 0)$ precisely when the energy drops strictly below C_2.

Here we see a wide neck at L_1, the L_2 has become a fixed point, and that L_3, L_4, and L_5 are still completely unaccessible. When the energy drops below C_2 we expect a second neck to open, allowing orbits near the Moon to move
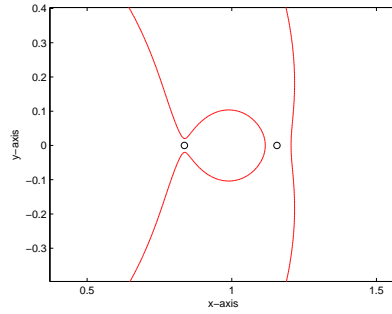
Figure 5: Zero velocity curve at $C_1 + 0.1(C_2 - C_1)$
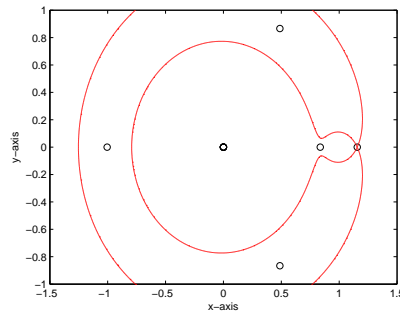
Figure 6: Zero velocity curve at C_2

away from the center of mass. Now there exists at least the possibility that some orbit beginning near the earth may escape the system all together. (At the same time, such an orbit may not exist. We only note the new possibility. The proof or disproof of such an orbit would certainly be an interesting result.)

In Fig(7) we see the energy surface for an energy smaller than C_2, and indeed a second neck has opened. Proceeding downward we have in Fig(8) the energy surface at C_3. As we should now have come to expect, there is yet another neck developing.

For energies less than C_3, motion is possible between the Earth and the Moon, out away from the center of mass, and there are two possible ways to renter the vicinity of the earth. From a topological point of view the opening at L_3 is no minor occurrence. Lets observe that prior to the appearance if this last neck, the space of allowable trajectories was either simply connected, or disconnected with simply connected components. (This is not completely true in the planar problem due to the singularities at the Earth and the Moon. However these singularities are still point singularities in the spatial **CRTBP**
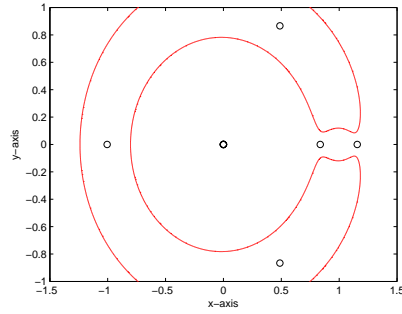
Figure 7: Zero velocity curve at $C_2 + 0.1(C_3 - C_2)$
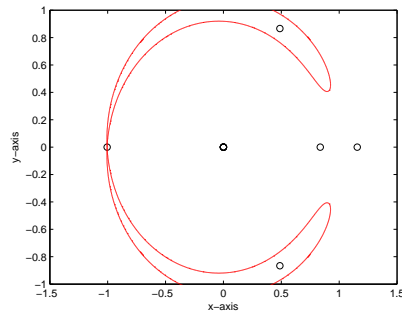
Figure 8: Zero velocity curve at C_3

and it may be posible to perturb around them. In any event the claim holds in the spatial problem.)

For energies above C_3 the only obstructions to an orbit being contractible in the plane are the singularities at the Earth and the Moon, but these are point obstructions. Once the neck at L_3 opens, a new possibility exists. If an orbit began near the earth, passed thought the neck at L_2 went around the Jacobi surface and returned to its initial state through the neck at L_3 (so that the orbit is periodic) then such an orbit would not form a contractible loop. Further contractibility could not be restored by a small perturbation into the spatial problem. This possibility is clearly seen in Fig(9)

When the energy is decreased further the upper and lower components will continue to shrink, until they finally disappear at $C_4 = C_5$. Now there are no forbidden regions as can be seen from Fig(10).

As another topological aside,consider how the homology of the (interior) of the Jacobi surface has changed. Initially it's interior was connected and there were (up to homology) two non-contractible one cycles. When the neck at L_1

28
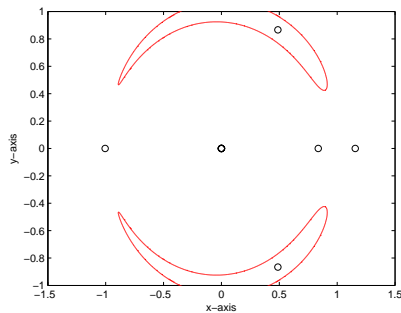
Figure 9: Zero velocity curve at $C_3 + 0.1(C_4 - C_3)$
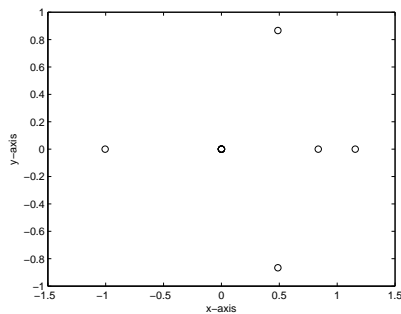
Figure 10: Zero velocity curve (or lack thereof)at C_4

formed, one of these cycles was destroyed (the one associated with the connected component of the Moon) but the other survived. When the neck at L_2 opened the second generator was destroyed as well, but the interior was still connected. The appearance of the neck at L_3 disconnects the interior, adding a generator to the zeroth homology. Finally when the energy reaches C_4 the surface completely disappears, taking all homology with it. Then the homology of the surface is related to the allowable orbits, and thus to the global dynamics of the system.

3.2   The Zero Velocity Surfaces in the Spatial Problem

Similar analysis can be done in the spatial **CRTBP**. Then each libration point will have two more eigenvalues and eigenvectors corresponding to the extra spatial dimensions. In fact all five libration points gain another complex conjugate pair of eigenvalues, and therefore two more eigenvectors in their center eigenspaces.

The zero velocity curves become surfaces in the full problem, and we examine

these surfaces here. As above we begin with the energy held just above the L_1 energy. The zero velocity surface is shown in Fig 11.
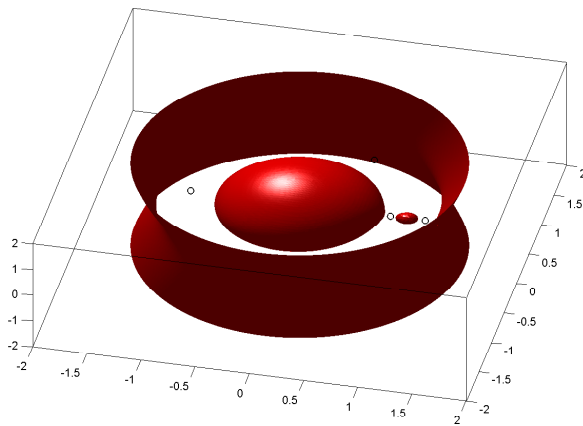
Figure 11: Zero velocity surface for energy above L_1

The surface is an non-compact, disconnected, smooth 2-manifold. This contrasts the planar case where the zero velocity curves (which are 1-manifolds) are always compact. It is often remarked that while the manifold is not a surface of revolution it's compact components can be roughly visualized by rotating the zero velocity curves from the planar problem about the x-axis.

At this energy level the Earth and Moon are each contained a sphere. An particle which orbits one can never reach the other, nor does it have any opportunity to become unbounded. These orbits are separated from the from the unbounded component of the phase space by an unbounded hyperbolic sheet, outside of which we have no guarantee that orbits must remain bounded. (It's an interesting question as to wether all orbits in this problem remain bounded at various energy levels. One expects that parabolic and hyperbolic orbits from the two body problem may continue into the **CRTBP** but we do not address this here. We are only trying parse the global information provided by the zero velocity surface).

Lowering the energy level to between that of L_1 and L_2 gives the image in Fig 12, where we have taken a closer view of the vicinity of L_1 as this is where the action is.

For energy levels below that of L_1 a neck opens up in the spatial problem just as in the planar problem, and it will now be possible for particles to travel back and forth between the vicinity of the Earth and the Moon. The phase space is still separated into bounded and unbounded regions by the hyperbolic surface, and the surface can at least proscribe rough dynamical possibilities of orbits near the Earth and Moon.
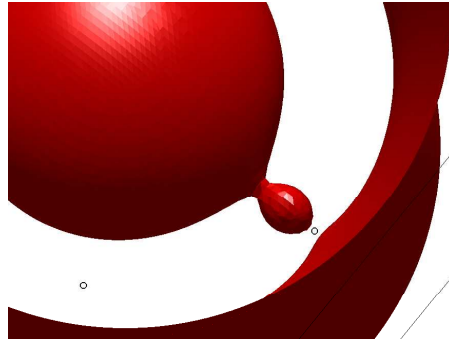
Figure 12: Zero velocity surface for energy between L_1 and L_2

This brings up an interesting point, which applies here as well as to the planar problem. Often in dynamical systems theory one begins by assuming that the phase space is a connected manifold, or at least a connected topological space. But here is a practical problem where this is not the case. The phase space is disconnected, but nevertheless the dynamics in one component is in some sense effected by the presence of the other. It's possible for a particle to orbit the Earth/Moon system from the outside of the hyperbolic surface, in the unbounded component of the phase space. Such a particle is effected by the presence of the Earth and the Moon, even though it can neve reach these points.

Of course one can think of the dynamics in the unbounded component in terms of just the vector field there, forgetting that the field is due to the presence of masses in another component. It's an interesting state of affairs nonetheless.

As we lower the energy below the level at L_2 we see in Fig 13 that a second neck opens at L_2, forming a connection between the sphere about the Moon and the unbounded component of the phase space.
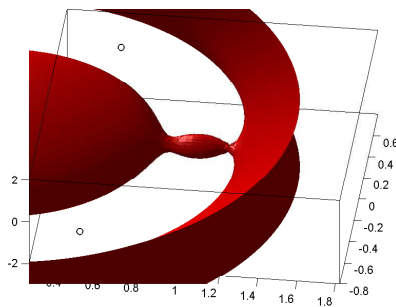
Figure 13: Zero velocity surface for energy a little below L_2

31

Indeed, now the phase space is connected and the surface can no longer tell us wether any orbits are bounded. An orbit near the Earth might pass to the vicinity of the Moon through the L_1 neck and from there after going through the neck at L_2 might escape the vicinity of the Earth Moon System entirely, perhaps even escaping to infinity. Orbits which come from infinity and fall into orbit around either the Earth or the Moon are possible as well.

As in the planar problem, lowering the energy below that of L_3 brings about a dramatic change in the phase space, as seen in Fig 14.
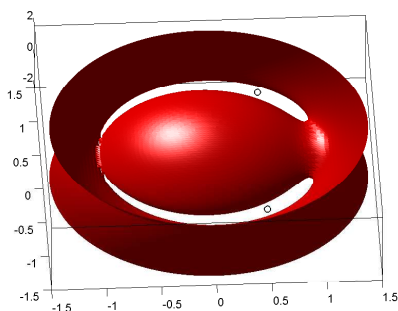
Figure 14: Zero velocity surface for energy a little below L_3

A third neck opens at L_3 changing again the global connectedness properties of the phase space. Also note that the necks at L_1 and L_2 have opened up into one large neck about the Moon, and the sphere around the Moon has flattened out entirely. This might suggest periodic and pseudo-periodic orbits about the Moon will be less common (at least for larger amplitudes), that capture near the Moon will be even more delicate, and that it will be easier for a particle orbiting the Earth to escape the Earth/Moon system.

For energies such as this, between L_3 and L_4, the phase space is not simply connected. This was discussed in detail with regards to the planar problem, but here we see a nontrivial cycle in the planar problem cannot be trivialized by going into the spatial problem. The nontrivial homology of the planar problem caries over into the spatial problem unchanged; it is not a peculiarity of the planar problem.

An nice illustration of this is shown in 15
Here the green star is the Moon and the red star is the Earth. The black circles near the Moon are L_1 and L_2 and we can see the neck (now looking aptly like a saddle) around the Moon clearly. On the other side of the Earth the last black circle is L_3 and the white gap is it's neck. The fact that we can see through these two necks gives hope that we could find an orbit which passed through. If an orbit could go all the way through, could there be periodic which do so? Such a periodic orbit would not be contractible (would in fact be a generator of the second homology group of the phase space).
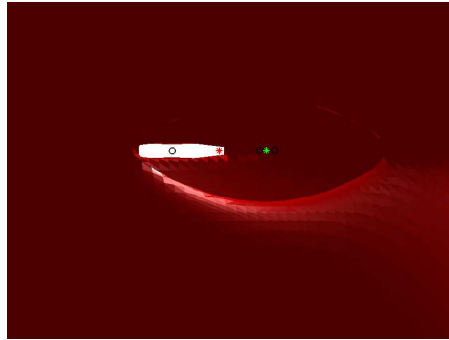
Figure 15: Through both necks; the Earth, Moon and the collinear libration points in one view

Finally we come to the case of energies below that at L_4. Here the spatial case differs somewhat from the planar. Recall that in the planar system the zero velocity curve vanished all together at the $_4$ energy level, and does not exist for energies below it. It can, however be seen in Fig 16 that while the energy surface recoils from the xy plane, it does not vanish altogether (this being said the obstruction to connectedness is gone).
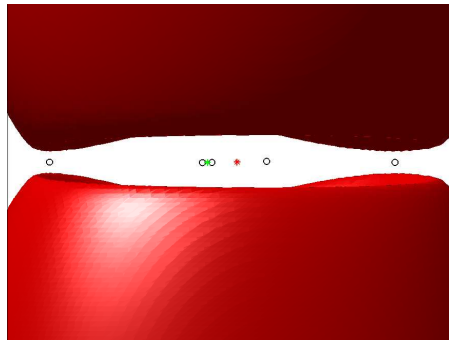
Figure 16: Zero velocity surface for energies below

Again the green is the Moon and the red is the Earth. This view is from the opposite side from the view in Fig 15. Now we are close to L_3, with the Moon and the other two collinear libration points on the far side of the Earth. The triangular libration points are the black circles on the left and right of the figure.

It's clear that the zero velocity surface is playing a smaller and smaller role in the dynamics of the system as the energy lowers (initial velocity increases). At this point it only tells us that orbits about the Earth cannot have too large an amplitude in the z direction, and that orbits which come into the vicinity of

the Earth from outside the Earth/Moon system must do so via orbits which are close to in-plane as they approach.

At high enough energy levels even this restriction will become negligible. This is as it should be though, as a fast enough trajectory (fast relative to the frequency of the orbit of the second primary about the first, or either primary about their center of mass) will pass by the Earth/Moon system without being deflected very much at all (unless it passes very near one of the primaries). In other words the distance of the surface from the primaries tells us a little about the effect the primaries have on orbits which begin far away yet pass near the Earth/Moon system at some point.

4 Numerical Experiments and Global Dynamics

The last section examined in some detail the possible local dynamics at the libration points by considering the linearized vector field there. We also considered certain obstructions to the global dynamics due to the Jacobi surface at varying energy levels. These considerations allow us to say that certain trajectories were and were not possible, but we have yet to see any actual orbits. This state of affairs will be remedied presently. This section will be primarily graphical. The main purpose is to present a "zoo" of orbits that actually do occur in the **CRTBP**, in order to complement our extensive list of things that cannot happen.

4.1 Orbits at Energies Between L_1 and L_2

In the first series of examples we set the Jacobi constant at $C = 3.18$, so that the neck at L_1 is open, but the necks at L_2 and L_3 are closed. Then motion between the Earth and Moon is not ruled out, but any orbit beginning in near either of the primaries must remain in the compact component of the phase space (the component containing the center of mass).

Our first orbits are rather tame. Figures (17) and (18) show, in rotating coordinates, two orbits which begin near the Earth or Moon, respectively, and seem to stay in orbit around them.

The initial positions for these orbits are

$$
\begin{aligned}
x_0 &= -0.75 \\
y_0 &= 0.0 \\
z_0 &= 0.0 \\
u_0 &= 0.0 \\
v_0 &= 1.0 \\
w_0 &= 0.0
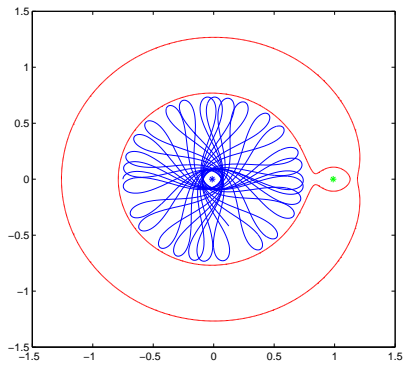\end{aligned}
$$

and

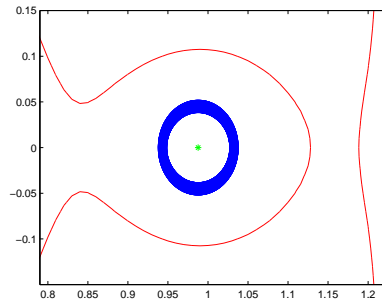Figure 17: An orbit which stays bound to Earth

Figure 18: An orbit which stays bound to the Moon

$$
\begin{aligned}
x_0 &= -0.75 \\
y_0 &= 0.0 \\
z_0 &= 0.0 \\
u_0 &= 0.0 \\
v_0 &= 1.0 \\
w_0 &= 0.0;
\end{aligned}
$$

The first trajectory orbits in the counter clockwise direction, contrary to the orbit of the Moon. The second orbit orbits the Moon and is also counter clockwise, but in this case the motion is retrograde, which has a stabilizing effect and causes a much more regular motion. Each orbit was integrated to $t_f = 48$, or approximately four years.

The orbits are shown in inertial coordinates in Figures (19) and (20).
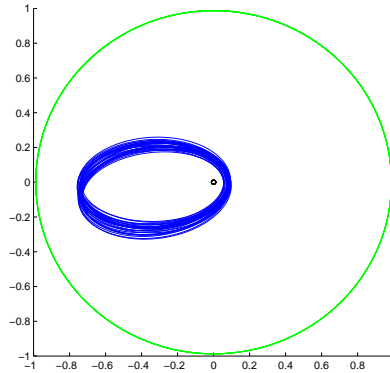
Figure 19: Earth orbit in inertial frame
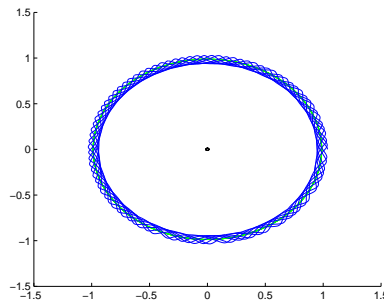
Figure 20: Orbit of the Moon in inertial frame

In both inertial plots the green line is the orbit of the moon and the earth makes a very small circle about the center of mass in the middle of the picture.

A closeup of the lunar orbit is shown in Fig(21)

The orbit is planar, and the particle does not collide with the Moon, so we see that the trajectory is passing ahead and behind the Moon, over and over again.

4.2   A Ballistic Capture Orbit

Next we present an orbit which is significantly more complicated. The energy level is still held at $C = 3.18$, but now we want an orbit that begins near the
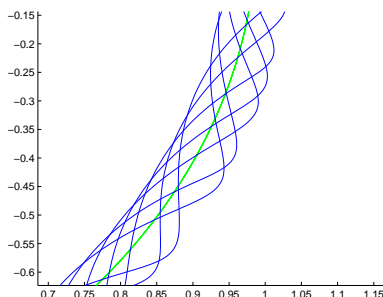
Figure 21: closeup of the lunar orbit

earth, passes through the neck at L_1, orbits the Moon several times, and then returns into an Earth orbit. In fact the orbit we present will complete this cycle no less than 6 times.

To find the desired orbit we begin with initial conditions

$$
\begin{aligned}
x_0 &= 0.83 \\
y_0 &= 0.0 \\
z_0 &= 0.0 \\
u_0 &= 0.5 \\
v_0 &= 1.0 \\
w_0 &= 0.0;
\end{aligned}
$$

near L_1. The trajectories there are very sensitive to initial conditions and it is hoped that by playing with the initial data a an orbit with the desired trajectory could be found. Once an orbit is found which goes from the Earth side of L_1 to the Moons, the orbit is integrated backwards to get it to the vicinity of the Earth. Taking this as a new initial condition and integrating forward forward gives an orbit which starts near the Earth and goes around the Moon.

If the system is integrated this way for a short time (forward and backward with $f_f = 15$ in both cases) we get the pictures in Figures (22) and (23) In these figures we see that the trajectory begins on the Earth side of L_1, passes a few times around the earth and then heads through the neck and into orbit around the moon, as desired.

The difference between the inertial and non-inertial frame is stark. The orbit seems messy and jarring in the inertial frame, while ordered and symmetrical in the rotation coordinates. Furthermore, it's hard to imagine how one would find such an orbit in the inertial frame, while in the rotating frame it is not difficult.

If we integrate the system longer an even more interesting picture develops. In Figures 24 and 25 the same orbit is integrated forward and backward until
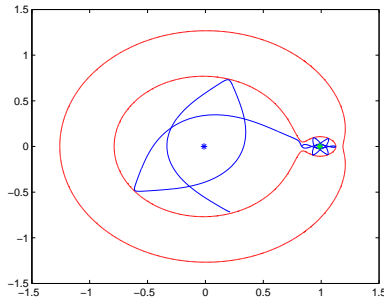
37

Figure 22: transfer orbit in rotating frame

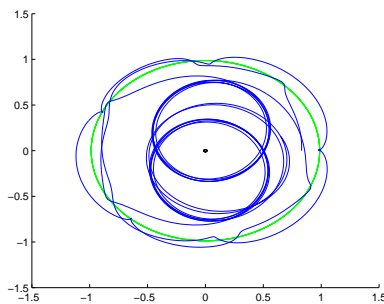
Figure 23: transfer orbit in inertial frame

$t_f = 280$, or for a total or 560 time units. The resulting orbit again seems very structured in the rotating frame, and much less so (at least near the Moon) in the inertial frame.

But the really interesting property of this orbit is highlighted if we examine the up of the neck near L_1 as shown in Fig(26). Here we see many crossings through the neck. Consider the obvious statement that the projectile is always on one side of the neck or the other, and that the neck at L_3 is closed. Then each line counts a transfer between the Earth and the Moon and once the projectile has passed from the Earth to the Moon, it remains on the moon side until the next crossing through the neck.

All this is obvious but the point is that associated to each crossing from the Earth to the Moon, either there is a crossing back to the Earth, or the projectile stays by the Moon. Then by counting the number or neck crossings, we get a count of how many transfers have been made; i.e. one transfer for each pair.

Carefully examining the plot shows that there are 13 crossings, and hence 6 transfers. The longer this trajectory was integrated, the more crossings were
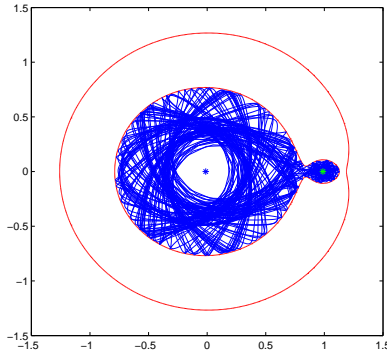
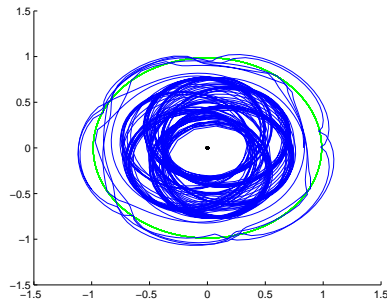Figure 24: long integration of the transfer orbit: rotational frame

Figure 25: long integration of the transfer orbit: inertial frame

found. It seems possible, and even likely, that this trajectory will oscillate between the Earth and Moon forever.

4.3 A 'There and Back Again' Orbit

Now decrease the energy to $C = 3.17$ so that the neck at L_2 opens, and it is possible to escape the the vicinity of the of the Earth-Moon system. Note however that escape is only possible through a small window; the neck at L_2. Here we want to find an orbit which begins near the Earth, goes through the L_1 neck into orbit around the Moon, leaves the L_2 neck and orbits the entire Earth-Moon system several times (or at least once) from outside the system and then returns to the neck at L_2, orbiting first the Moon again, and then returning to the vicinity of the earth.

To find such an orbit we consider the most demanding requirement first; to
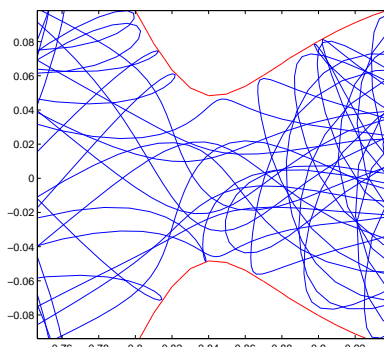
Figure 26: transfer orbit in inertial frame

leave the energy surface, wind nontrivially around the center of mass (origin) and then return. As with the previous problem we begin by looking at orbits which begin near L_2. Again, the system should be more sensitive here, since we are on a saddle, and we have a much better chance of finding this behavior here than we would have if we simply began with initial conditions near the Earth.

By taking an initial condition just to the right, and slightly below $L_2 =$ we can find orbits that leave the vicinity, orbit the system for a while, come back in and seem to "strike" the energy surface, bouncing off it again. By tweaking the initial conditions and integrating for longer and longer blocks of time we can actually get the projectile to "bounce" of the energy surface several times. (Zooming in it's clear that the particle does not strike the zero energy surface, but comes almost to a stop complete stop and then falls behind the still rotating system, but the imagery helps more than it hurts).

By further varying the parameters it is seen that the locations of the "impacts" with the zero velocity curve can be moved. By adjusting the initial state yet more we are able to get the projectile to strike right at the L_2 neck, and since there is an opening here, it goes right back in.

Now that an initial condition which starts near L_2, leaves, orbits the system and comes back has been found, the initial condition can be integrated backwards, and hopefully it goes back into the neck. This is why we started looking near, but just below and to the right of the second libration point; it is hoped that most orbits that end up there came from inside the neck. Indeed with a little luck this is what happens and we find the desired orbit.

The initial condition obtained after integrating backward by 20 time units is

$$
\begin{aligned}
x_0 &= 0.30910452642073 \\
y_0 &= 0.07738174525518
\end{aligned}
$$

40

$$
\begin{aligned}
z_0 &= 0.0 \\
u_0 &= -0.72560796964234 \\
v_0 &= 1.55464233412773 \\
w_0 &= 0.0;
\end{aligned}
$$

which is indeed on the Earth side of L_1. Now we integrate this forward, confident that the trajectory so obtained will exhibit the desired behavior. In all the description below, the claim that an orbit has $t_f = \tau$, means that it is integrated from the above state to time zero (when it is just past L_2) and then from time zero to time τ, making the total duration of the orbit $\tau + 20$ time units.

Figure 27 shows the trajectory integrated to time $t_f = 15$. The projectile begins at the state above (to the right and slightly above the earth) and orbits the Earth roughly ten times before a near flyby of L_1 and on to the Moon. It swings around the Moon twice before leaving the primaries through the L_2 neck. (This brings us up to time zero, at which time the projectile is very close to but just below and to the right of L_2 as described above).
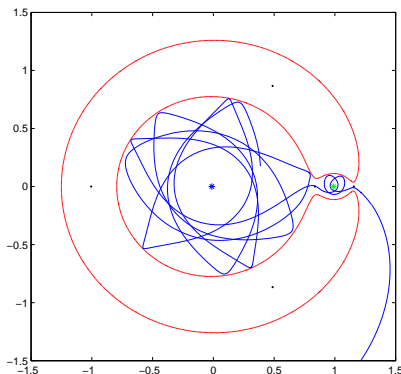

Figure 27: Itinerary: begins at earth, leaves through L_2 gap

The projectile leaves the system and we must change scales to continue to follow it. In inertial coordinates we see the trajectory shown in Fig 28.

Now the orbit looks very regular near earth, almost periodic, until it jumps tangentially off the ellipse to the Moon. After this follows an irregular, staggering trajectory around the Moon before a violent "bounce" off the orbit of the Moon which ejects the projectile from the system.

The projectile remains ejected for some time persists for some time. The exit was at roughly time zero. A look at the system in the rotational coordinates at time $t_f = 77$ Fig 29 Shows that the projectile has orbited the system from, mostly from a distance, though once "striking" the zero velocity curve on its lower right side.
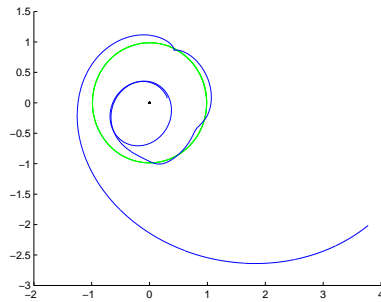
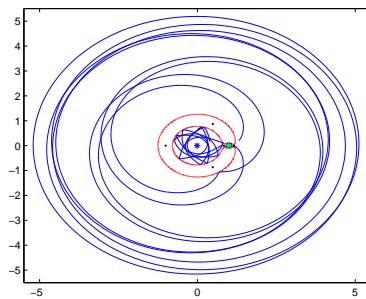Figure 28: Itinerary: beginning of trip, inertial frame

Figure 29: Itinerary: at time $t_f = 77$ is still outside

A closer look at this same picture shows that the projectile is returning to the neighborhood of the L_2 neck Fig 30.

Next, the two figures Fig 31 and Fig 32 show the projectile passing back through the neck above L_2 , preforming a double flyby of the Moon, and heading toward L_1

The next plot shows the trajectory having passed L_1 and returned to the vicinity of Earth (Fig(33)).

The last two plots show the entire trip plotted in inertial coordinates.

Note in these last three plots again how regular the inertial trajectory looks when it seems to be orbiting the Earth. Both it's near earth orbits and it's distant orbits seem to be almost elliptical, near periodic orbits. But when the influence of the moon becomes strong enough to pull the projectile away from these earth orbiting ellipses and onto the Moons path, the inertial orbit seems highly irregular, lurching , and crooked. On the other hand it is exactly when the projectile is under the Moons influence that its motion seems the most regular in the rotational frame.
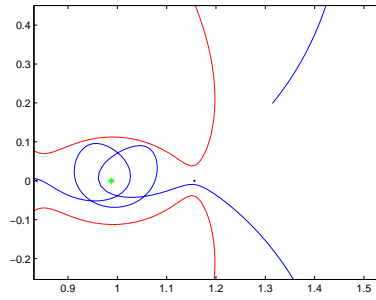
42

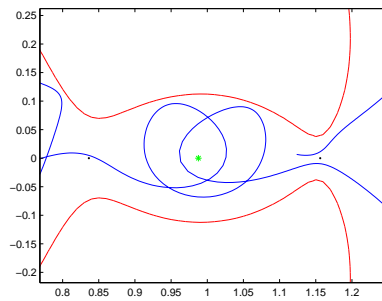Figure 30: Closer Look: projectile coming home

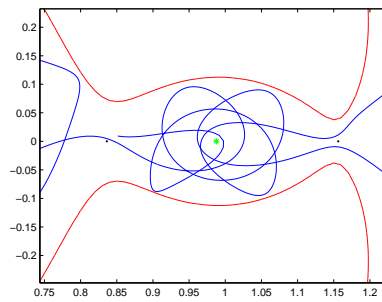

Figure 31: Through the door at L_2

Figure 32: Approaching L_1 and heading to Earth

It is also worth noting that it would have been much more difficult to find these orbits in inertial coordinates. There is simply not enough geometric struc-
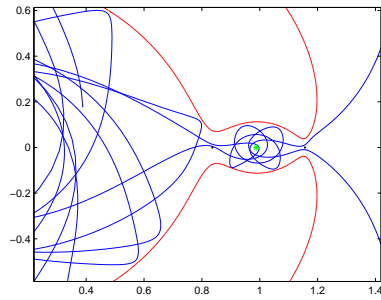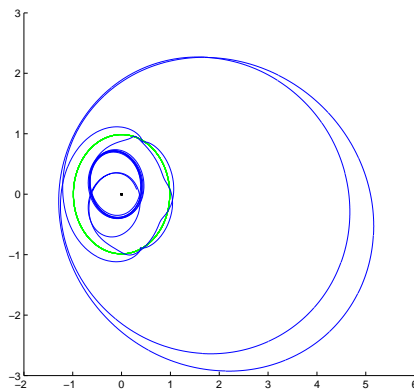
Figure 33: The completed itinerary

Figure 34: The completed itinerary; inertial frame

ture to tell you where to get started. Yet in the rotational system one can, simply by trial and error, locate orbits with a great variety of prescribed behavior, and by simple inspection rule out the existence many other orbits with certain properties.

Hopefully these examples give an impression of the rich orbit structure here. Combining our earlier negative analysis with the 'zoo' of orbits, gives significant insight into the possible dynamics in this problem. The next section builds on linear analysis at the libration points to increase our understanding of the local dynamics there, and to obtain some additional global information.
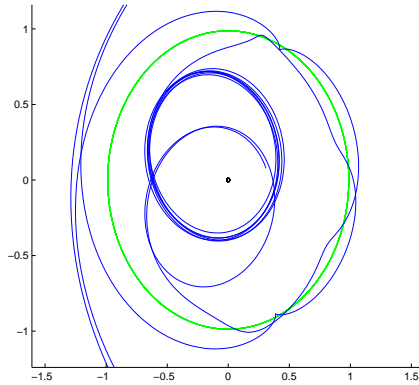
Figure 35: The completed itinerary; inertial frame close up

5 Numerical Study of the Linear and Nonlinear Dynamics Near L_4 and L_1 in the Earth-Moon System

In earlier sections the equations of motion for the linear dynamics about the libration points were developed. In this section we use these dynamics to find orbits with desirable properties in the linear system, and then by appropriate change of coordinates see if there are orbits with similar properties in the nonlinear system.

5.1 Linear Flow Near a Fixed Point

We recall from linear systems theory ([HS], [MH]) that a matrix can always be brought into the Jordan Canonical form where it is diagonalized by it's eigenvalues and generalized eigenvalues. For the systems matrix of the linearization of the **CRTBP** at any of the libration points the matrix will in fact have distinct eigenvalues so we assume this.

Then given the system

$$\dot{\mathbf{x}} = A\mathbf{x}$$

With initial conditions $\mathbf{x_0}$. We can write

$$\dot{\mathbf{x}} = TDT^{-1}\mathbf{x}$$

where T is the matrix of eigenvectors and D is the diagonalized matrix of eigenvalues.

45

Consider the ivertable linear transformation $T^{-1}\mathbf{x} = \mathbf{y}$. The matrix T^{-1} is constant so we have that

$$\dot{\mathbf{y}} = (T^{-1}\mathbf{x})' = T^{-1}\dot{\mathbf{x}}$$

so that

$$
\begin{aligned}
\dot{\mathbf{x}} &= TDT^{-1}\mathbf{x} \\
\dot{\mathbf{x}} &= TD\mathbf{y} \\
T^{-1}\dot{\mathbf{x}} &= D\mathbf{y} \\
\dot{\mathbf{y}} &= D\mathbf{y}
\end{aligned}
$$

with initial conditions $\mathbf{y_0} = T^{-1}\mathbf{x_0}$. This last system is diagonalized, and hence decoupled and we can write down the flow directly. This is

$$\mathbf{y}(t) = e^{Dt}\mathbf{y_0} = \begin{pmatrix} e^{\lambda_1 t} & \dots & 0 \\ \vdots & \ddots & \vdots \\ 0 & \dots & e^{\lambda_n} \end{pmatrix} \mathbf{y_0}$$

where this form of the exponential is only valid as we have assumed the system is diagonalized. Transforming this flow back to the original coordinates gives

$$\mathbf{x}(t) = Te^{Dt}T^{-1}\mathbf{x_0}$$

Another useful trick that can aid in the global analysis of a linear system is to ignore the initial condition $\mathbf{x_0}$, and consider the system matrix D. This is diagonalized, and so it's dynamical behavior is easily parsed. Briefly, the eigenvalues with $Re(\lambda) < 0$ give rise to stable solutions, $Re(\lambda) > 0$ unstable solutions and $Re(\lambda) = 0$ oscillatory solutions.

Then in the $\mathbf{y}$ system we can easily choose solutions with some desired behavior by choosing $\mathbf{y_0}$ to mute certain modes and amplify others. Once the right linear combination of initial conditions gives the desired behavior we can transform these initial conditions to the original domain, and the transformed solution will have the same properties (probably embedded differently).

5.2 Linearized Dynamics at L_4

Consider the linearized dynamics about L_4 in the earth Moon system. We will use the coordinates $\mathbf{x} = (x, y, u, v)$ for the physical variables in the linear system, $\mathbf{x}'$ for the physical variables in the nonlinear system, and $\mathbf{y} = (y_1, y_2, y_3, y_4)$ for the variables of the diagonalized system. If we simulate the linear and nonlinear systems from the same physical state, we have to remember that the origin in the linear system corresponds to the point $(L_1, 0, 0, 0)$ in the nonlinear system. Then the $\mathbf{x}$ coordinates should be thought of as displacements from the equilibrium, and the $\mathbf{x}'$ coordinates are the physical variables for the circular restricted three

body problem. To start the nonlinear system and the linearized system from the "same" physical point we use $\mathbf{x}_0$ as initial conditions for the linear system and $\mathbf{x}'_0 = (L_1, 0, 0, 0) + \mathbf{x}_0$ for the initial conditions in the nonlinear equations.

This notation runs the risk of being slightly confusing, but keeps with the notion established above. We just note that y without a $1, 2, 3$ or 4 subscript is the second component of $\mathbf{x}$, while y_i will always be a component of $\mathbf{y}$ when $i = 1, 2, 3, 4$.

We know the eigenvalues of the linearized system at L_4 are

$$
\begin{aligned}
\lambda_1 &= -0.95396766945875i \\
\lambda_2 &= 0.95396766945875i \\
\lambda_3 &= -0.29990946238396i \\
\lambda_4 &= 0.29990946238396i
\end{aligned}
$$

so there are two frequencies and all solutions are linear combinations of harmonic motion. Consider the behavior of the the linear and nonlinear systems begun with initial conditions (displacement from equilibrium) $\mathbf{x_0} = (0.001, 0.001, 0.0, 0.0)^T$. The resulting trajectories are shown in Fig(37). Here the linear system integrated with the initial condition $\mathbf{x}_0$ while the nonlinear system is integrated with the condition $\mathbf{x}'_0 = L_4 + \mathbf{x}_0$. The two trajectories are plotted in the same figure with the linear in red and the nonlinear in blue (of course the linear trajectory has to be shifted to be centered at L_4 in order for the plots to match up).
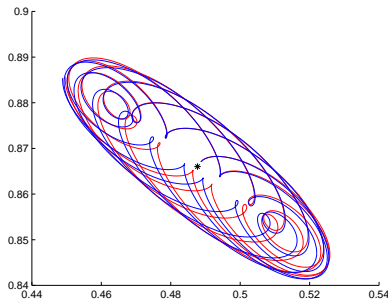

Figure 36: Linear and Nonlinear orbits; same initial conditions

This orbit is integrated for roughly ten years and we see that the linear and nonlinear orbits agree both qualitatively and qualitatively throughout the integration.

Now suppose instead of specifying an initial condition for the system we want to find an orbit near near L_4 with some prescribed behavior, say an orbit with only one frequency. Well, for the diagonalized system this is easy. We will choose the slow mode with frequencies $\omega = 0.29990946238396$ and want an

amplitude of $A = 0.005$, so as to stay close to the region where the linearized and the original dynamics are strongly correlated (we hope; the results will validate this).

So, since we want to kill the fast mode we begin with an initial $\mathbf{y_0}$ of the form $(0, 0, y_3, y_4)$ where the non-zero entries may be complex. In fact, if we want real solutions in the $\mathbf{x}$ coordinates we should either do another coordinate change, or take y_3 and y_4 to be complex conjugates. Then (partly to show that using complex y is completely acceptable) we choose

$$y_3(0) = 0.0025(1 + i)$$

and

$$y_4(0) = 0.0025(1 - i)$$

which is roughly the desired magnitude and will give harmonic motion with only the slow frequency. Transform these initial conditions to the original domain, i.e the $\mathbf{x}$ variables. The transformation is

$$\mathbf{x}_0 = T\mathbf{y}_0$$

which gives

$$
\begin{aligned}
x_0 &= -0.00410832055367 \\
y_0 &= 0.00327788247585 \\
u_0 &= 0.00123212420855 \\
v_0 &= -0.00035138543034
\end{aligned}
$$

We simulate these initial conditions in both the linear and nonlinear systems for ten periods. The results are fig(37) and fig(38).

From these we see that we certainly found a single mode oscillation in the Linear model. In the nonlinear problem, the same initial conditions seem to lead to quasi periodic motion, still bounded near L_4 and qualitatively similar to the linear solution.

5.3 Linearized Dynamics at L_1

The linearized dynamics at L_1 (or any of the collinear libration points for that matter) have a stable and an unstable direction, and a four dimensional center (two dimensional in the planar problem). Then the long term dynamics near L_1 will be qualitatively quite different form those seen above near L_4.

Specifically, The center eigenspace is tangent to the center manifold of the nonlinear problem but the two spaces intersect only at the equilibria. We expect the linearized dynamics to approximate the nonlinear in a small neighborhood of the equilibrium and, in fact, for a small enough neighborhood and short time,
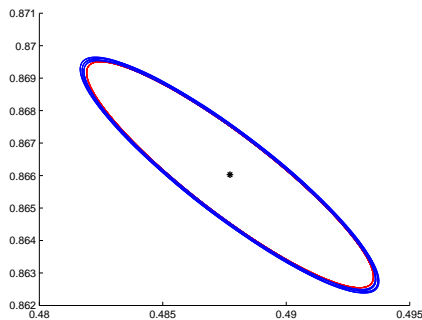
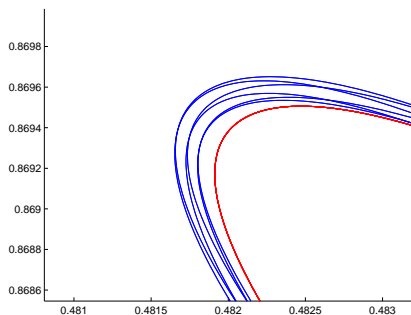Figure 37: Linear and Nonlinear orbits; one mode of oscillation

Figure 38: Linear and Nonlinear orbits; Closeup

the approximation may be quite good. Nevertheless, since the tangent space and the center manifold will (probably) not completely coincide in any neighborhood of the equilibrium, a nonzero vector in the center eigenspace which evolves under the nonlinear dynamics will have some (probably small) component in either the stable or unstable direction.

If this component is small then the nonlinear behavior will mimic the linear behavior for a long time. (The time may be approximated by comparing the expansive and contractive time constants to the magnitude of the component in the unstable or stable directions, but this involves actually knowing how the center manifold embeds near the equilibria). Eventually however the small stable or unstable component will come to dominate the behavior, as they are associated with exponential growth, or contraction. We repeat the numerical experiment from the previous section at L_1 in order to see clearly these effects.

As in the case at L_4 we begin by considering a small displacement from the equilibrium $\mathbf{x_0} = (0.001, 0.001, 0.0, 0.0)^T$ in the linear system and $\mathbf{x'_0} =$

49

$(L_1, 0, 0, 0) + (0.001, 0.001, 0.0, 0.0)^T$ in the nonlinear system. The results of the integration are shown in 39.
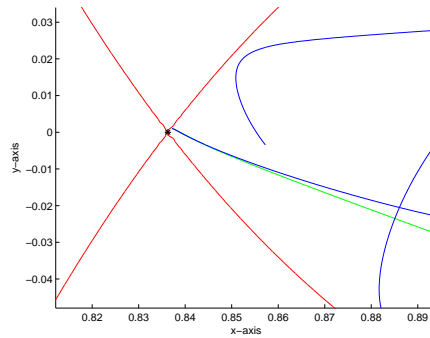

Figure 39: Linear and Nonlinear orbits; Closeup

The figure gives a close up on the neighborhood of L_1. The blue orbit is the nonlinear trajectory. The linear is green, while the zero velocity curve for the initial conditions is shown in red, and the black star is L_1. We can see that the two trajectories begin at the same point, and begin to move off in the same direction. This state of affairs persists only for a short time however, as by the edge of the figure the trajectories are beginning to diverge.

If we allow the simulation to continue for several periods (say four) of the linear system, then we see that globally, the dynamics of the linear and nonlinear systems loose all correlation, in marked contrast to the situation at L_4. Fig 40 illustrates this.
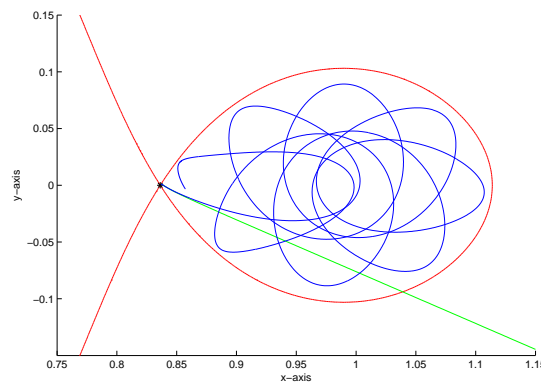

Figure 40: Linear and Nonlinear orbits; Global View

Again, we see that the trajectories agree for some time near the beginning of the experiment, but then diverge completely. Here the difference between linear and nonlinear behavior is stark. Before making further comment on this, we transform the initial conditions for the linear system into the diagonalized coordinates. Doing this we get $\mathbf{y}_0 = T^{-1}\mathbf{x}_0$;

$$
\begin{aligned}
y_1(0) &= 0.00168962454824 \\
y_2(0) &= 0.00237644988143 \\
y_3(0) &= -0.00090794385517 - 0.00119655578224i \\
y_4(0) &= -0.00090794385517 + 0.00119655578224i
\end{aligned}
$$

Recall that the eigenvalues at L_1 are

$$
\begin{aligned}
\lambda_1 &= 2.93362180133508 \\
\lambda_2 &= -2.93362180133508 \\
\lambda_3 &= 2.33537262850117i \\
\lambda_4 &= -2.33537262850117i
\end{aligned}
$$

so the linear initial condition has nonzero component in the linear unstable direction. Then it's global behavior must be unbounded.

Contrast this with the behavior of the nonlinear orbit. For this energy level the neck at L_2 and hence L_3 are closed. Then without reservation, we can sat the nonlinear trajectory is bounded. We see that the global behavior of the linear trajectory tells us nothing about the global behavior of the nonlinear system, which highlights the local nature of the linear analysis.

Suppose now that we try to minimize the component in the unstable direction of the nonlinear trajectory. To do this choose initial conditions which correspond to harmonic motion of the linear system in a ball of radius 10^{-6} about the fixed point, and compar the resulting behavior in the nonlinear system in the same neighborhood. The center space of the linear system must be tangent to the center manifold of the nonlinear system at the fixed point. But, as of yet we do not have estimates of the size of the neighborhood on which this "best linear approximation" remains valid.

Since we want to stimulate only the harmonic mode of the linear system, take the initial condition;

$$
\begin{aligned}
y_1(0) &= 0 \\
y_2(0) &= 0 \\
y_3(0) &= 10^{-4}(0.5 + 0.5i)0 \\
y_4(0) &= 10^{-4}(0.5 - 0.5i)
\end{aligned}
$$

in the diagonalized system. Transforming these conditions back to the physical coordinates gives

$$
\begin{aligned}
x_0 &= 0.0 \\
y_0 &= -10^{-4}0.37917672785887 \\
u_0 &= -10^{-4}0.24680494811508 \\
v_0 &= 0.0
\end{aligned}
$$

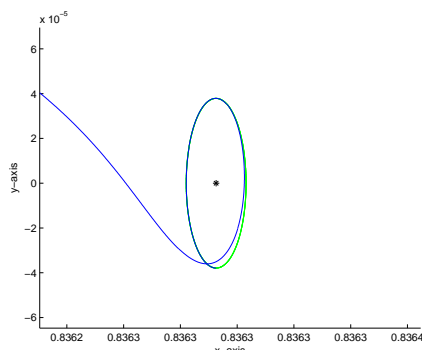which we integrate in both the linear and nonlinear models. The results are in Fig 41.

Figure 41: Linear and Nonlinear orbits; Linear Harmonic Case

Again the blue is the nonlinear orbit and the green is the linear. Clearly we have taken a small enough neighborhood that the local, short time agreement between the linear and nonlinear systems is good. The green orbit for the linear dynamics has been chosen to be periodic. The blue nonlinear trajectory, with the same initial conditions begins tangent to the linear curve and furthermore follows the linear orbit for almost one full period.

However, it will again be stressed that this agreement is completely local. The global picture is shown in 42 and highlights this difference.

To see the long term behavior of the nonlinear trajectory we must choose a spatial scale which makes the linear orbit invisible. Further while the linear orbit exhibited harmonic motion (it was an ellipse), it is clear that this is not so of the nonlinear trajectory which is in all likelihood not even periodic.

Nevertheless the linear analysis at L_1 can be made to yield global results. The nonlinear orbit does come close to closing in on itself, which suggests that there may be a periodic orbit nearby (we may be able to close this orbit).

In fact we can find one beginning at $(0.001, 0)$ in the configuration space, an order of magnitude farther from L_1 than we were in the last examples.

First we'd like to begin with an initial condition which has $x_0 = 0.001, y_1 = 0$ and gives harmonic motion in the linear model. This is the same position which gave the results in Figs 39 and 40, and we begin with them only to show that you can.
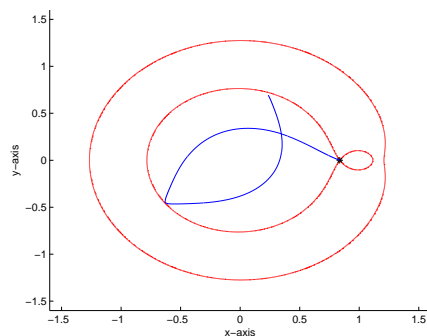
Figure 42: Linear and Nonlinear orbits; global picture

In the diagonalized model we want to mute the stable and unstable modes. If we choose complex conjugate intimal conditions which are purely imaginary in the **y** system, then we obtain initial conditions in the **x** linear system which are harmonic and such that $y_0 = 0$. As we saw above, purely imaginary complex conjugate initial conditions in the diagonalized system transform to physical initial conditions with zero x_0 component. Similarly, real complex conjugate initial conditions in the diagonalized system transform to physical initial conditions with $y_0 = 0$. Choosing such a vector and normalizing so that $x_0 = 0.001$ we have that the condition

$$
\begin{aligned}
y_1(0) &= 0.0 \\
y_2(0) &= 0.0 \\
y_3(0) &= 0.00473121111697 \\
y_4(0) &= 0.00473121111697
\end{aligned}
$$

in the diagonalized domain and

$$
\begin{aligned}
x_0 &= 0.001 \\
y_0 &= 0 \\
u_0 &= 0 \\
v_0 &= -0.00837915421626
\end{aligned}
$$

for the physical coordinates. These conditions have been chosen to mute the stable and unstable eigenvectors and must give harmonic motion in the linear system. Clearly they satisfy the $x_0 = 0.001$, $y_0 = 0$. Integrating them gives the picture in Fig 43.
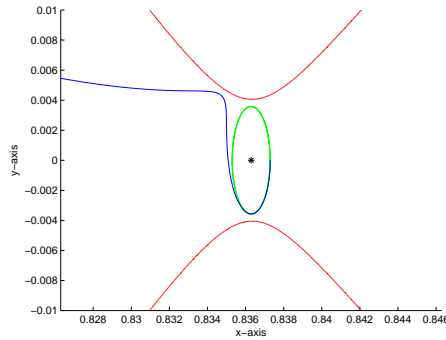
53

Figure 43: The new orbit sitting in the L_1 neck

This time the linear orbit is of the same scale as the opening at L_1. Again the nonlinear orbit agrees with the linear orbit for a short time, but then falls into the earths influence.

However we hope that by adjusting the initial velocity (which has only z component) we will be able to find a periodic orbit in the nonlinear model with the same position coordinates, sitting in the L_1 neck.

Note that in Fig 43 when the nonlinear trajectory leaves the linear orbit, it diverges to the left. A little experimentation shows that a small increase in the initial velocity (say adding 0.0001 to v_0) causes the nonlinear trajectory to diverge to the right, where it goes into orbit around the moon.

This switching is good news. If it's possible to find some orbits which fall to the left, and some that fall to the right, we hope that somewhere in between this behavior bifurcates, and at the critical velocity falls neither to the left nor the right. An orbit which neither falls to the left nor the right would be periodic (or at least quasi periodic) and remain bound to the neighborhood of L_1.

Adjusting the initial velocity by hand, raising it a little if the trajectory diverges to the left, lowering it if it diverges to the right, gets the nonlinear orbit to stay on the linear orbit for longer and longer. After a few minutes we settle on the velocity adjustment $\Delta v_0 = 0.00006100116814757635 8748755$. Here all figures but the last are significant, in the sense that adjusting any digit down will cause the orbit to diverge to the left rather than the right, and raising any digit will result in the trajectory diverging on the right as shown. (Of course at this many figures one suspects that the results are routine dependant). The resulting trajectory is shown in Fig 44

The simulation has run for roughly four periods of the linear frequency. Note that the linear orbit follows agrees with the nonlinear orbit very well for at least three and a half cycles, and begins to diverge just before coming back to meet itself for the forth time. For perspective, one period is roughly 2.33 time units, while 2π time units is a (lunar) month in this system. Then our projectile has
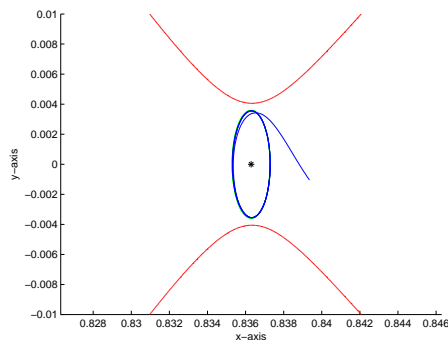
Figure 44: Unstable Periodic Orbit Near L_1

orbited L_1 for roughly two months; a nontrivial mission in people time.

The difference between the original initial conditions, and the conditions leading to the 'periodic' orbit are on the order of 10^{-2}. So the periodic orbit is not too far from the initial conditions.

Of course, truth be told, we certainly have not proven there is a periodic orbit at L_1 in the nonlinear system. These results merely suggest the existence of one. The exercise shows that we seem to be able to get the nonlinear orbit to stay near L_1 (and the linear orbit) for longer and longer times by adjusting the initial conditions. Nevertheless after tuning the perturbation to 26 decimal places we can still only manage four periods of agreement. Contrast this to the experiment at L_1 where, in the absence of an unstable manifold, the linear and nonlinear orbits remain near one another indefinitely.

This also highlights the limitations of such course numerics, and indicates the need for more sophisticated methods. Ones which could in fact prove what seems so intuitively clear; that there is in fact a periodic orbit here in the nonlinear system.

Then working with the linear model has finally yielded a least a global conjecture; that there are periodic orbits about L_1 near the harmonic orbits in the linear model. More than that, we have a method for actually computing them. In fact wether they exist or not, this experiment seems to show that for all practical purposes (where only finite times can matter) we can design missions which orbit the collinear libration points for months, and have significant amplitude. (The orbit shown here has almost maximal amplitude, in the sense that it is almost the full size of the L_1 neck).

Remark: The reader familiar with this problem is aware that the orbit which sits in the neck is a Lyapunov orbit, and does indeed continue from the linear problem to the nonlinear one.

6   Poincare Maps

Another tool we want to present in the context of the circular restricted three body problem is Poincare Maps. Poincare maps can give a much more global picture of the dynamics of a system than the linear analysis presented above, and are certainly a much more systematic tool than the "messing around" method of earlier sections.

To construct a Poincare Map one often begins with a fixed point $\mathbf{x}_0$, or a periodic orbit P, and a codimension one surface Σ which should be taken transverse to the flow (assume that Σ is smooth. In fact, near P we can simply take Σ to be a plane normal to P). In a Hamiltonian system restricting to an constant energy level allows a further reduction of the dimension.

For $\mathbf{x}_1, \mathbf{x}_2 \in \Sigma$ define a new mapping $f : \Sigma \to \Sigma$ by $f(\mathbf{x}_1) = \mathbf{x}_2$ if $\phi(\mathbf{x}_1, \tau(\mathbf{x}_1)) = \mathbf{x}_2$ where $\tau : \Sigma \to \mathbb{R}^+$ is defined to be the "first return time" of the of the trajectory $\phi(\mathbf{x}, t)$ to the surface Σ. Explicitly

$$\tau(\mathbf{x}) = \inf_{T > 0} \phi(\mathbf{x}, T) \in \Sigma$$

If the origin of the mapping is taken to be $O \equiv P \bigcap \Sigma$ then $\tau(O)$ is defined as P is periodic. Then an implicit function argument shows that τ is well defined, and as smooth as the flow, on some neighborhood of the orbit.

As will be discussed more in the next set of notes, the monodromy matrix for P has two unity eigenvalues; one in the direction of the flow, and one in the direction of change in energy. If we disregard these, the remaining eigenvalues are the eigenvalues of the differential of f_c, which is the Poincare map, restricted to the energy level c associated with P. Then the monodromy matrix describes how orbits near P behave.

Poincare maps are a fundamental tool in the dynamical systems toolkit for analyzing flows. Judicious choice of Poincare map reduces the dimension of the system by at least one. Furthermore it can be shown that the flow is topologically semi-conjugate to any of it's Poincare maps. Then the discrete dynamical system generated by the Poincare map gives a lower bound on the complexity of the dynamics of the flow. Period points in the poincare map expose periodic orbits in the flow. Similarly for mixing, or chaotic behavior, or ergodicity, or any dynamical property one wishes to consider.

What's more the local constructions described above can often be extended numerically to produce Poincare maps on larger domains. These can give significant insight into the orbit structure of a dynamical system as we will see.

6.1   Maps in the CRTBP

The phase space of the planar **CRTBP** is 4 dimensional, and certainly difficult to visualize. It is not only convenient but quite natural to restrict the energy to a particular value and consider the resulting dynamics on the energy manifold.

An autonomous Hamiltonian system always has an integral, and trajectories at different energy levels cannot interact; unless the system is somehow

perturbed trajectories do not change energy levels. Then it makes sense to consider the dynamics in different energy surfaces as different dynamical systems. When considered in these terms a Hamiltonian vector field does not give rise to one dynamical system, but to a sheaf of them.

In any event it is quite reasonable to examine the planar **CRTBP** at fixed energy levels, in which case it is a three dimensional continuous time dynamical system. However, since the resulting system still preserves phase volume (on the energy surface) we don't expect attractors or repellers (in fact these cannot exist). Then the flow in this three dimensional space will be quite recurrent, and the orbit structure may still be very difficult to visualize.

Restricting further to a Poincare map in a fixed energy manifold gives a two dimensional discrete time dynamical system, and our eyes can aid us in the analysis of the dynamics. In the spatial problem the same strategy leads to a four dimensional Poincare map, so it's less clear how to proceed in the full problem. Nevertheless we will find that some of what we learn about the planar dynamics will be valuable when the spatial problem is taken up in the next set of notes.

The computer program 'CRTBPmap2.m' builds the Poincare map for the the **CRTBP**. We take μ for the Earth/Moon system and integrate 3000 initial conditions along the x axis between $-\mu + 0.005$ and $L_1 + 0.01$. All initial conditions begin with no initial x velocity and a positive y velocity whose magnitude determined by the energy level, which is set at $C = C_{L_1} - 0.5(C_{L_1} - C_{L_2})$. The initial conditions are integrated for 50 time units and interpolated to $150,000$ points per orbit.

The first 25 data points per orbit are ignored, and the rest are searched for crossings of the xz-plane, with positive y derivative. A point is considered to be on the xz-plane when $|y| < 0.0001$. When such a point is found, the program skips 25 data points and continues the search.

At the crossing of the xz plane, the x, $\dot{x}$ and ϕ coordinates are saved, where ϕ is angle between the velocity vector and the x axis modulo 2π. In fig 45 the map is shown with $33,778$ points plotted.

The result is a global Poincare section for the **CRTBP**. The x axis ranges over from $-\mu$ to L_2 (the Earth is the red star near zero, and the green star on the far right is the earth). Remember that only the x variable is a physical coordinate and that the vertical axis is the x component of velocity. The scale of the Poincare map shown here is the scale of the system.

Anyone who has ever looked at Poincare maps for 'chaotic' dynamical systems with strange attractors, such as the Lorenz or Rosseler systems, will note that this is qualitatively a very different picture. In those systems the phase space dissipation pulls all trajectories to the attractor (which can only exist in a dissipative system). To build a Poincare map in a dissipative system one can often get away with integrating only one trajectory but for a very long time. In a system with an attractor which supports ergodic dynamics a generic trajectory is dense on the attractor and hence tells the whole story.

Not so here. There seem to be ergodic components, but they are separated from each other by other kinds of behavior. In any event, it is not the case that
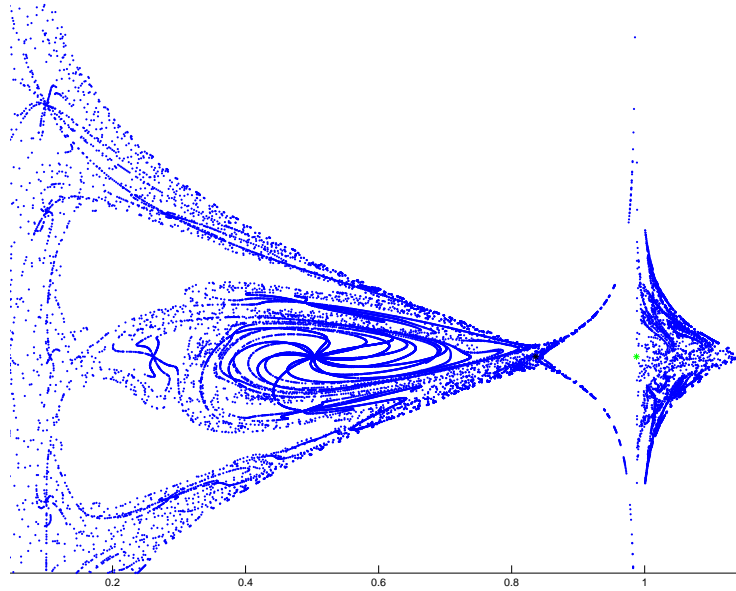
Figure 45: Global Poincare Section; x versus $\dot{x}$

a generic orbit will, if integrated long enough produce the picture we see here. In the **CRTBP** it is necessary to take a much larger sample of the phase space.

Lets put this discussion aside for a moment and return to the purpose of this experiment, which is to gain a better understanding of the dynamics of the **CRTBP**. Has the mapping given us any new information? Lets pick some interesting looking points on the map, and see what kinds of orbits they correspond to.

A most striking feature seems to be the activity near the x axis at about $x = 0.6$. By zooming in on this nexus we estimate the initial conditions in the center to be $x = 0.50455$, and $\dot{x} = 0$. From this information we can recover the entire initial state in phase space, as the energy is prescribed at $C = 3.17315916582532$. Then the magnitude of the velocity is determined by the Jacobi integral, and we have $|\mathbf{v}| = 0.97697707489055$. But the Poincare map was defined for crossings with $\dot{y} > 0$. Then the full initial condition is roughly

$$\mathbf{x}_0 = \left(\begin{array}{c} 0.50455 \\ 0.0 \\ 0.0 \\ 0.0 \\ 0.97697 \\ 0.0 \end{array} \right)$$

Integrating these conditions forward gives the orbit in fig 46.
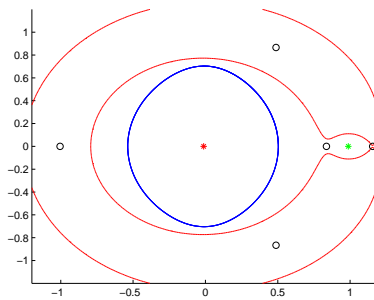

Figure 46: Orbit generated by center of 'nexus'

In the rotating frame, this is a periodic orbit around the earth. It orbits in a counterclockwise fashion. This picture was generated by integrating the conditions for 25 time units. That the trajectory remains on this curve suggests strongly that the orbit is stable. Especially as we simply 'eye-balled' the initial conditions from the Poincare map; no Newton steps were done here to guarantee periodicity.

Then it's a little more clear what is going on in this 'nexus' now. There is a fixed point of the Poincare map in the center on the nexus. The fixed point is a stable center (purely imaginary eigenvalues). The 'tendrils' we see in fig 45 emanating from the fixed point are due to a strobing effect, and not due to trajectories escaping from the fixed point. If we wee to integrate each trajectory longer these would fill out into invariant circles. As it is, we are only catching roughly 10 points per circle and then moving to another orbit. This is causing the strobing.

To test this hypothesis, we zoom in on an initial condition on one of these invariant circles. Integration it forward should give a trajectory which is dense in a 2-torus. The initial condition we choose is

$$\mathbf{x}_0 = \begin{pmatrix} 0.50455 \\ 0.0 \\ 0.0 \\ 0.0 \\ 0.97697 \\ 0.0 \end{pmatrix}$$

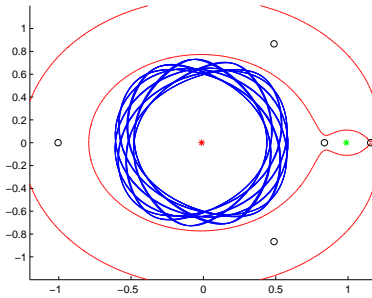which is far removed from the fixed point itself, but well within the nexus.

Figure 47: Orbit generated by center of 'nexus'

This leads to the orbit in fig 47. The figure suggests that we have found the correct interpretation of the Poincare map. The orbit certainly seems to fill more space than a periodic orbit, while remaining bounded roughly between two circles in the configuration space (and we guess that it stays on a torus in the phase space). The conditions were integrated for 200 time units which lends credence to conjecture that the orbit is in the center of the fixed point.

Now that we have a better understanding of how to read the Poincare map, lets have a closer look at the region around the nexus. This is shown in fig 48

Now we see that there are what seem to be other fixed (periodic?) points of the Poincare map about the first one, each with it's own center. Choosing the one almost directly about the first fixed point we find the coordinates

$$\mathbf{x}_0 = \begin{pmatrix} 0.491 \\ 0.0 \\ 0.0 \\ 0.545 \\ 0.863419 \\ 0.0 \end{pmatrix}$$

Here the x and $\dot{x}$ coordinates are read off the Poincare map. The magnitude of the velocity is determined by the energy which gives the $\dot{y}$ component by the Pythagorean theorem.
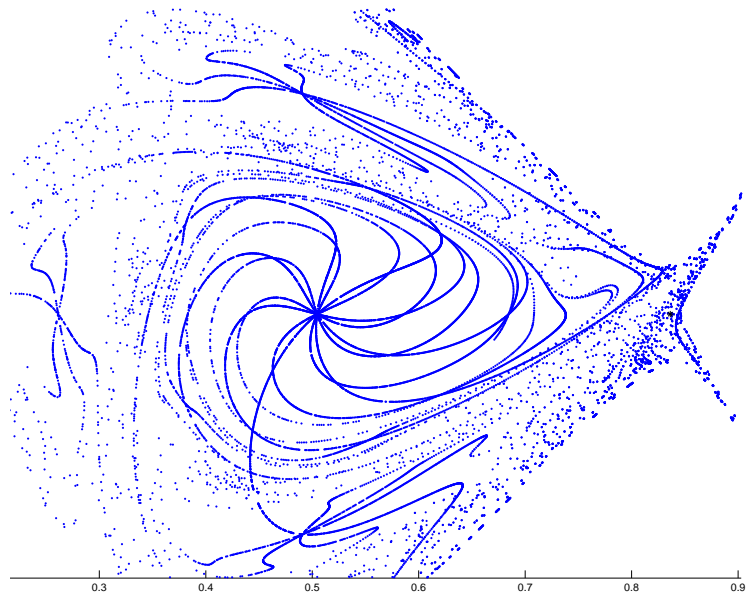
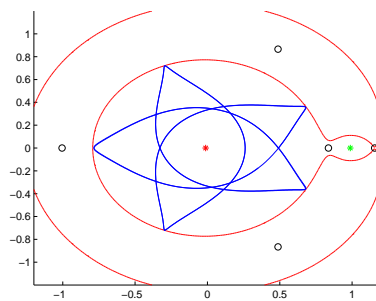Figure 48: Poincare section close up

Figure 49: Another periodic orbit from the Poincare map

Again, the orbit is stable, and we could use coordinates on the invariant circles of the Poincare map near the fixed point to find orbits which are dense on the boundary of a tubular neighborhood of this orbit.

Looking back at the original Poincare map (fig 45) we see another periodic orbit in the top left hand corner. If we work out the initial conditions for this

61

orbit we obtain the stable periodic orbit shown in fig 50.
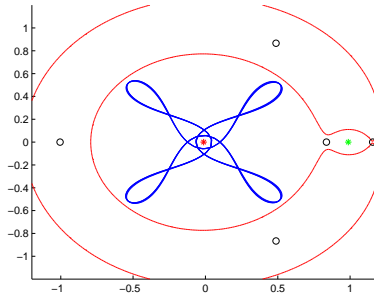

Figure 50: More periodic orbits

It seems clear that we could play this game all day. With finer Poincare maps perhaps there is no end to the number of distinct periodic orbits we could find. In fact, if we use our imaginations a little, it looks as though this Poincare map has the features of the 'solenoid' mapping of Smale. (Stretching and folding a torus into itself infinitely many times).

Can we get more from the map? So far we have picked orbits where the Poincare map seems close to integrable, in the sense that it should have action angle coordinates near the fixed points. (The spiraling of the tendrils near the fixed points is consistent with the mapping being a twist map near the fixed points). Can we get interesting non-periodic orbits from the map?

If the **CRTBP** is not completely integrable, then we expect that away from the fixed points, we may be able to find 'chaotic islands' where the systems dynamics is mixing, and extremely sensitive to initial conditions. These regions would look more like white noise in the Poincare map.

There do seem to be such regions in our mapping. Consider fig 48 again. There are clearly fixed points near $x = 0.5$ and $x = 0.25$ both on the x-axis, and both seem to have local centers. But closer to 0.34 the behavior looks like it could be 'noisier'.

Such an orbit is shown in fig 51. We see that the orbit wanders. It begins as thought it is near an invariant torus of a periodic orbit of the earth. Then it strays off thought the L_1 neck and seems to shadow another invariant torus near the moon. This kind of transport is suggestive of Chaos.

A time series for this orbit is shown in fig 52, and while graphical evidence in never enough to conclude the existence of chaos, this is as noisy a waveform as one could hope to see. Especially interesting is the wobble on the top of the crest between roughly $t = 90$ and $t = 100$, which is due to the ballistic capture of the projectile by the moon.

Is the orbit sensitive to small perturbations in the initial conditions? To see, we perturb the conditions in the fifth decimal place and integrate again. The
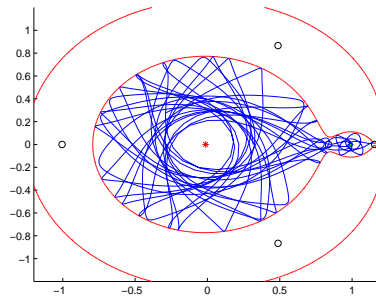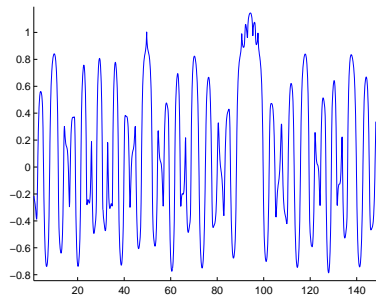
Figure 51: chaotic trajectory?

Figure 52: Time versus the x component of the capture trajectory
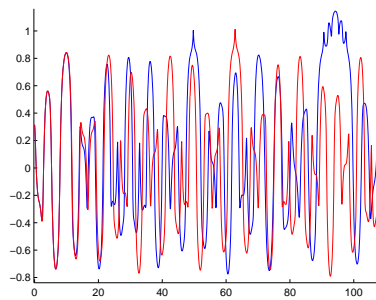
results are in fig 53.

Figure 53: Sensitive to initial conditions

63

This is the calling card of sensitivity to initial conditions. The orbits begin by shadowing one another perfectly from time $t = 0$ to $t = 15$, begin to move apart at $t = 20$, and are uncorrelated by time $t = 70$. We can see that at $t = 90$ when the first particle is captured by the Moon, the perturbed trajectory remains near the Earth.

The divergence of trajectories from one another is related to the concept of Lyapunov exponents. It's interesting then to note that in some regions of the phase space, say near the fixed points and periodic orbits of the Poincare map, the Lyapunov exponents can be neutral, and nearby initial conditions can remain correlated for arbitrarily long times. While in other parts of the phase space, say in the chaotic islands, the Lyapunov exponents can drive initial conditions apart quickly.

Again, this is in contrast to what one usually sees in dissipative systems where the phase space is often initially contracted to the attractor, where the expansive Lyapunov exponents take over, driving trajectories apart. In other words, a more uniform treatment of the initial conditions is common. This non-uniformity in the phase space is part of what makes Hamiltonian systems so rich.

At any rate, we have definitely seen how the Poincare maps can inform our understanding of the global dynamics of the problem. Unfortunately (fortunately?) our eyes are not as helpful in higher dimensions, and other methods must be devised in order to get information from the Poincare sections.

References

[C2] C. Ocampo, The Lagrange Equilateral Solution for the G3BP, Unpublished Notes

[C2] C. Ocampo, The Euler Straight Line Solution for the G3BP, Unpublished Notes

[A] Methods of Applied Mathematics, Unpublished Notes: www.math.utexas.edu/ arbogast/

[C] Alain Chenciner, Richard Montgomery, " A Remarkable periodic solution of the three-body problem in the case of equal masses", Annals of Mathematics, 152 (2000), 881-901

[Ch] Ward Cheney, Analysis for Applied Mathematics, Springer

[G] Marian Gidea, Clark Robinson, "Symbolic Dynamics for Transition Tori-II", Qualitative Theory of Dynamical Systems 1, 1-14 (2000) Article No.1

[HS] Morris W. Hirsch, Stephen Smale, Differential Equations, Dynamical Systems, and Linear Algebra, Academic Press

[MH] K.R. Meyer, G.R. Hall, Introduction to Hamiltonian Dynamical Systems and the N-body Problem, Springer-Verlag

[M] Richard Montgomery, "A New Solution to the Three-Body Problem", Notices of the AMS, May 2001, 471-481

[Nah] Paul J. Nahin, An Imaginary Tale: The Story of $\sqrt{-1}$, Princeton University Press, 1998

[R] Clark Robinson, Dynamical Systems: Stability, Symbolic Dynamics, and Chaos, Second Edition, CRC Press, Boca Raton Florida, 1999